NASA Technical Memorandum 84563

Analysis of Oscillatory Motion of a Light Airplane at High Values of Lift Coefficient

James G. Batterson
Langley Research Center
Hampton, Virginia

National Aeronautics
and Space Administration

**Scientific and Technical
Information Branch**

1983

SUMMARY

A modified stepwise regression is applied to flight data from a light research airplane operating at high angles of attack. The well-known phenomenon referred to as "bucking" or "porpoising" is analyzed and modeled using both power series and spline expansions of the aerodynamic force and moment coefficients associated with the longitudinal equations of motion. The resulting models are validated by numerically integrating them using initial flight conditions and flight control inputs. In addition, a one-degree-of-freedom Van der Pol model is used to help explain the oscillatory behavior, and the possible existence of hysteresis in the lift curve is demonstrated.

INTRODUCTION

An analysis of airplane flight data which exhibits seemingly spontaneous short-period longitudinal oscillations occurring at high values of C_L is presented. Such behavior has popularly been referred to as "bucking" or "porpoising." Phillips (ref. 1) developed several possible models to simulate such behavior on the hybrid computer. His models involved hysteresis loops in the aerodynamic force and moment coefficients in the region of maximum lift. Other authors (refs. 2 and 3) have developed models for self-excited longitudinal motion in the deep-stall condition. This paper addresses another example of bucking or porpoising behavior. Oscillations were encountered at high values of C_L by a light airplane modified specifically for high α operation. A published report (ref. 4) on wind-tunnel tests of a model of a similar (but smaller) airplane with the same modification indicates that maximum lift is at a significantly higher angle of attack. By applying a stepwise regression technique to flight data from a nonlinear operating regime of a light single-engine research airplane, mathematical models are synthesized and aerodynamic parameters are evaluated. Two methods, one utilizing partitioning or binning of the data, and the other employing spline basis functions, are used in the model structure determination and parameter estimation process. A brief description of each method is contained herein. In addition, the Van der Pol equation is used to help illustrate and explain the oscillatory motions of the airplane. The flight data are also analyzed in an effort to detect possible hysteresis in the lift curve.

A better understanding of nonlinear aerodynamic phenomena and the analysis of such phenomena are important in aviation safety and in the synthesis of flight control laws for nonlinear operating regimes (ref. 5).

SYMBOLS

a_X, a_Y, a_Z acceleration along longitudinal, lateral, and vertical body axes, respectively, g units

b span, m

C_L lift coefficient, $L/\bar{q}S$

$C_{L,max}$ maximum lift value of lift coefficient, $L/\bar{q}S$

C_l	rolling-moment coefficient, $M_X/\bar{q}Sb$
C_m	pitching-moment coefficient, $M_Y/\bar{q}S\bar{c}$
C'_m	defined in appendix
C_n	yawing-moment coefficient, $M_Z/\bar{q}Sb$
C_X	longitudinal-force coefficient, $F_X/\bar{q}S$
C_Y	side-force coefficient, $F_Y/\bar{q}S$
C_Z	vertical-force coefficient, $F_Z/\bar{q}S$
c.g.	center of gravity
$\bar{c}$	mean aerodynamic chord, m
F	F-statistic
F_p	F-statistic used in partial F-test
F_X, F_Y, F_Z	force along longitudinal, lateral, and vertical body axes, respectively, N
g	acceleration due to gravity, m/sec^2
I_X, I_Y, I_Z	moment of inertia about longitudinal, lateral, and vertical body axes, respectively, $kg-m^2$
I_{XZ}	product of inertia, $kg-m^2$
J	cost function
K	number of spline knots
L	lift, N
M_X, M_Y, M_Z	rolling, pitching, and yawing moments, respectively, N-m
m	mass, Kg
N	number of data points
p	body axis roll rate, rad/sec or deg/sec
q	body axis pitch rate, rad/sec or deg/sec
$\bar{q}$	$= \frac{1}{2}\rho V^2$, dynamic pressure, Pa
R^2	squared multiple correlation coefficient
r	body axis yaw rate, rad/sec or deg/sec

S	wing area, m^2
$s^2(\theta_j)$	variance of parameter estimate, θ_j
t	time, sec
u	component of velocity along longitudinal body axis, m/sec
V	total airspeed, m/sec
v	component of velocity along lateral body axis, m/sec
w	component of velocity along vertical body axis, m/sec
x_j	jth element of n × 1 vector of independent variables
y	n × 1 vector of dependent variables
z	dummy variable
α	angle of attack, rad or deg
α_i	value of angle of attack corresponding to ith spline knot, rad or deg
$(\alpha - \alpha_i)_+^m$	$\equiv \begin{cases} (\alpha - \alpha_i)^m & (\alpha > \alpha_i) \\ 0 & (\alpha < \alpha_i) \end{cases}$
β	angle of sideslip, rad or deg
$\Delta\alpha$	$= \alpha - \alpha_o$, rad or deg
$(\Delta\alpha)_{crit}$	difference between trim angle of attack and angle of attack at which pitch damping changes sign
δ_a	aileron deflection, rad or deg
δ_e	stabilator deflection (positive for trailing edge down), rad or sec
δ_r	rudder deflection, rad or deg
ε	damping coefficient in Van der Pol differential equation
θ	pitch angle, rad or deg
Θ	(n + 1) × 1 vector of unknown parameters
θ_j	jth element of vector of unknown parameters
ρ	air density, kg/m^3
ϕ	bank angle, rad or deg
ω_{osc}	characteristic oscillation frequency, rad/sec

Subscript:

o trim value

Superscripts:

• derivative with respect to time

^ optimal estimate

Derivatives:

$$C_{m_q} = \frac{\partial C_m}{\partial q\ \bar{c}/2V} \qquad C_{m_{q\alpha}} = \frac{\partial^2 C_m}{\partial q\ \partial\alpha\ \bar{c}/2V} \qquad C_{m_\alpha} = \frac{\partial C_m}{\partial\alpha}$$

$$C_{m_{\dot\alpha}} = \frac{\partial C_m}{\partial\dot\alpha\ \bar{c}/2V} \qquad C_{m_{\delta_e}} = \frac{\partial C_m}{\partial\delta_e}$$

$$C_{m_{\delta_e\alpha}} = \frac{\partial^2 C_m}{\partial\delta_e\ \partial\alpha} \qquad C_{m_{\beta^2}} = \frac{1}{2}\frac{\partial^2 C_m}{\partial\beta^2} \qquad C_{m_{\beta^2\alpha}} = \frac{1}{2}\frac{\partial^3 C_m}{\partial\alpha\ \partial\beta^2}$$

$$C_{m_{\alpha^i}} = \frac{1}{i!}\frac{\partial^i C_m}{\partial\alpha^i} \qquad (i = 2, 3, \ldots, 8)$$

$$C_{Z_q} = \frac{\partial C_Z}{\partial q\ \bar{c}/2V} \qquad C_{Z_{q\alpha}} = \frac{\partial^2 C_Z}{\partial\alpha\ \partial q\ \bar{c}/2V} \qquad C_{Z_\alpha} = \frac{\partial C_Z}{\partial\alpha}$$

$$C_{Z_{\delta_e}} = \frac{\partial C_m}{\partial\delta_e} \qquad C_{Z_{\delta_e\alpha}} = \frac{\partial^2 C_Z}{\partial\alpha\ \partial\delta_e} \qquad C_{Z_{\beta^2}} = \frac{1}{2}\frac{\partial^2 C_Z}{\partial\beta^2}$$

$$C_{Z_{\beta^2\alpha}} = \frac{1}{2}\frac{\partial^3 C_Z}{\partial\alpha\ \partial\beta^2} \qquad C_{Z_{\alpha^i}} = \frac{1}{i!}\frac{\partial^i C_Z}{\partial\alpha^i} \qquad (i = 2, 3, \ldots, 8)$$

$$C_{Z_{\sqrt{\dot\alpha}}} = \frac{\partial C_Z}{\partial\sqrt{\dot\alpha}\ \bar{c}/2V} \qquad C_{Z_{\sqrt{\dot\alpha}\,\alpha}} = \frac{\partial^2 C_Z}{\partial\alpha\ \partial\sqrt{\dot\alpha}\ \bar{c}/2V}$$

FLIGHT VEHICLE AND DATA ACQUISITION

The test-flight vehicle was a single-engine, low-wing, four-seat, light airplane. Flight control was provided by the throttle, stabilator (all movable tail), ailerons, and rudder. Flaps were available, but were not used in the tests considered in this report. The wing leading edge had been modified by extending the outboard half of each leading edge as indicated in figure 1 and in modification B for the model of a two-place airplane in reference 4. This was one of several leading-edge modifications that were made on this airplane to research the stall/spin characteristics of such a modified airplane. The flight data analyzed herein were obtained during standard stability and control parameter estimation flights. In these flights, the pilot attempts to trim the airplane to some steady-state reference flight condition from which he can initiate some perturbation by the movement of controls. All data analyzed in this report are assumed to have equilibrium initial conditions ($p = q = r = \dot{\alpha} = \dot{\beta} = \beta = v = \dot{w} = \dot{u} = 0$). Data were measured by rate gyros for roll, pitch, and yaw rates; roll and pitch angles were measured by attitude gyros. Angles of attack and side slip were measured by wind vanes mounted on booms on each wing tip as shown in figure 1. Linear accelerations were measured by accelerometers located close to the airplane center of gravity with three mutually orthogonal axes pointing in the directions of the longitudinal, lateral, and vertical body reference axes of the airplane. Control displacements were measured by potentiometers located close to the respective control surface so as to eliminate time delays and inaccuracies in the measurements of displacement due to control-cable stretch.

Data were recorded onboard the test airplane as analog voltage signals. The records of these voltages were filtered by a 6-Hz low-pass filter, and digitized to a sample rate of 20 per second after each flight. The digitized 20-sample-per-second data were then corrected for c.g. offset of the instruments, upwash and bias error on the wind vanes, and bias errors in the a_Z accelerometer and the angular-rate gyros.

ANALYTICAL PROCEDURE

System Identification

The system identification problem was defined by Zadeh (ref. 6) as "determination, on the basis of observation of input and output, of a system within a specified class of systems to which the system under test is equivalent." For the system identification of an airplane operating at low angle of attack, the mathematical model structure of aerodynamic forces and moments is linear. Hence, the identification problem reduces to a parameter estimation problem. However, at high angle of attack and in near-stall operating regimes, the form of the aerodynamic forces and moments must be determined before estimating corresponding parameter values. The general form of the mathematical model structure for the aerodynamic force and moment coefficients can be written as

$$y(t) = \theta_0 + \theta_1 x_1(t) + \theta_2 x_2(t) + \ldots \theta_n x_n(t) \qquad (1)$$

where

$y(t)$ aerodynamic force or moment coefficient ($C_X, C_Y, C_Z, C_m, C_l, C_n$) at time t

$x_j(t)$ airplane state plus control variables ($\alpha, q, \beta, p, r, \delta_e, \delta_a, \delta_r$) and their combinations at time t ($j = 1, 2, \ldots, n$)

θ_j airplane stability and control coefficients ($j = 1, 2, \ldots, n$)

θ_0 constant reflecting any initial steady-state condition

Thus, although it is assumed for the identification problem at low angles of attack that only first-order terms in the state and control variables are required for the model, the identification problem at high angles of attack can require terms such as α^2, α^3, $q\alpha$, and $\delta_e\alpha$. Hence, part of the identification problem is the proper choice of these higher-order terms for which parameters must be estimated. For example, consider the vertical-force coefficient C_Z. For the linear model,

$$C_Z = C_{Z_o} + C_{Z_\alpha}\Delta\alpha + C_{Z_q}\frac{q\bar{c}}{2V} + C_{Z_{\delta_e}}\Delta\delta_e \tag{2}$$

where $\Delta\alpha = \alpha - \alpha_o$ and $\Delta\delta_e = \delta_e - \delta_{e_o}$ for steady state ($v_o = p_o = q_o = r_o = \phi_o = 0$) initial flight conditions. A corresponding nonlinear model for high-angle-of-attack maneuvers might be written as

$$C_Z = C_{Z_o} + C_{Z_\alpha}\Delta\alpha + C_{Z_q}\frac{q\bar{c}}{2V} + C_{Z_{\delta_e}}\Delta\delta_e + C_{Z_{\alpha^2}}(\Delta\alpha)^2 + C_{Z_{\alpha_q}}\Delta\alpha\frac{q\bar{c}}{2V} \tag{3}$$

The specified class of models from which a nonlinear model may be chosen is given by the candidate model variables (table 1). Table 1 is a set of influence variables for longitudinal motion. The first column is simply the linear model variables α, q, and the linear control variable δ_e, on which the short-period longitudinal motion depends. The second column is the variation of the linear terms with changing angle of attack. The terms β^2 and $\beta^2\alpha$ in the third column allow for aerodynamic coupling to lateral motion, and the last column contains the terms allowing strong nonlinear variation with angle of attack, the main longitudinal independent variable. The list of variables in table 1 can be expanded or changed to investigate any particular behavior that is a function of α, q, and δ_e.

Once a class of candidate model variables is specified, the problem still remains to select the proper subset of that class. For the work described in this report, a semiautomated procedure, the stepwise regression, is employed. The stepwise regression parameter estimates are actually linear regression parameter estimates predicated on the minimization of the equation error, whose mean square is given by the cost function

$$J = \frac{1}{N}\sum_{i=1}^{N}[y(i) - \hat{y}(i)]^2 \tag{4}$$

where

$$\hat{y}(i) = \hat{\theta}_0 + \sum_{j=1}^{N} x_j(i)\,\hat{\theta}_j$$

and the values of $\hat{\theta}_j$ are the equation error optimal parameter estimates ($j = 0, 1, \ldots, n$). In the stepwise regression, the x_j's are added to the regression according to their effectiveness in reducing the equation error cost function J. This value is represented by the partial F value F_p of the coefficient as follows:

$$F_p = \frac{\hat{\theta}_j^2}{s^2(\hat{\theta}_j)} \tag{5}$$

where $\hat{\theta}_j$ is the estimate of θ_j and $s^2(\hat{\theta}_j)$ is the variance of $\hat{\theta}_j$. The value of the stepwise regression in system identification is that it not only selects a model from a large class of candidate model variables but it simultaneously estimates the corresponding parameters for that model.

When applying a stepwise regression to flight data, it should be remembered that the data are corrupted by measurement noise, and perhaps by process noise, which appears in the form of modeling error. Hence, the regression, with fewer independent variables than data measurements, always adds additional terms in order to reduce J. Though all these terms tend to fit the data better, some terms simply fit the noise. Hence, some criterion is needed to determine the point at which the adding of variables should cease. Experience has shown that several criteria should be employed to ensure an adequate model that fits the data, has good prediction capabilities, and makes sense physically. (See ref. 7.) These criteria include:

1. F_p should be greater than 5.

2. F should be a maximum.

3. R^2 should be close to 100 percent.

4. The residual sequence should be statistically equivalent to white noise. This determination is made by observing the autocorrelation function for the residual sequence.

No satisfactory single performance index has been written as a function of these separate criteria; hence, the selection of an adequate model is still somewhat subjective.

Partitioning of Data

It was demonstrated in reference 8 that for large-amplitude longitudinal maneuvers the partitioning of data as a function of angle of attack provided a finer resolution of stability and control parameters for the maneuver range than could be achieved by analyzing the entire data string intact. This partitioning, or binning, technique can be applied as follows. Consider a data set consisting of the measurements of several variables of 400 time points each. The time history of one such variable, α, is shown in figure 2. Several bins can be created, each containing data corresponding to a given range of α. The lines drawn parallel to the abscissa in figure 2 represent the bin boundaries. For example, all data corresponding to $0° \leq \alpha < 4°$ would be associated with the first bin, data for $4° \leq \alpha < 8°$ would be associated with the second bin, and so forth, as shown in figure 2. Then each bin,

which now contains data corresponding to a limited range of angle of attack, can be analyzed for aerodynamic stability and control derivatives corresponding to that angle-of-attack region.

There are, however, several problems associated with identifying parameters from binned data. The first is that by arbitrarily assigning bin widths, the α region may not be divided finely enough. However, one might also divide the region so that there are too little data in each bin for a proper analysis. Moreover, the location of the bin endpoints might obscure an important feature of the data if the endpoints were shifted a degree. Hence, a second technique was applied to the data in an attempt to alleviate these potential problems. This second technique allows the data to "bin itself" through the use of spline functions. This approach is more general in applicability than the simple binning and can be described as follows. The range of the independent variable which is most important in the determination of the dependent variable is partitioned into several subsets, each having support on less of the range than the previous subset. For example, the force coefficient C_Z is mainly dependent on α. Hence, if $\alpha = \{z | a \leq z \leq b\}$, then the α range, $[a,b]$, is divided according to the spline basis functions as follows:

$$(\alpha - \alpha_i)_+^m \equiv \begin{cases} (\alpha - \alpha_i)^m & (\alpha > \alpha_i) \\ 0 & (\alpha < \alpha_i) \end{cases}$$

The values of α_i are called knots. An example of the "+" function is given in figure 3. The four knots in this figure are at $\alpha = 2°$, $4°$, $6°$, and $8°$. Hence, $(\alpha - \alpha_1)_+^0 = 1$ for $\alpha > \alpha_1 = 2°$, and $(\alpha - \alpha_1)_+^0 = 0$ for $\alpha < \alpha_1$. Similarly, $(\alpha - \alpha_2)_+^0 = 1$ for $\alpha > 4°$, and $(\alpha - \alpha_2)_+^0 = 0$ for $\alpha < 4°$, and so forth, for the rest of the "+" functions. If the order of the "+" function, denoted by the superscript m is other than zero, say 2, then $(\alpha - \alpha_1)_+^2 = (\alpha - \alpha_1)^2$ for $\alpha > \alpha_1$ and $(\alpha - \alpha_1)_+^2 = 0$ for $\alpha < \alpha_1$. For the analysis in this paper, the knots were placed every 0.5° between $\alpha = 10°$ and $\alpha = 18°$. By placing knots every 0.5° and then allowing the stepwise regression to determine significant terms, the problem of choosing too narrow a bin in the binning technique is avoided. The longitudinal force and moment coefficients were then written as follows:

$$C_X = C_{X,o} + C_{X_\alpha}\alpha + \sum_{i=1}^{K} C_{X_{\alpha_i}}(\alpha - \alpha_i)_+ + C_{X_q}\frac{\bar{q}c}{2V} + \sum_{i=1}^{K} C_{X_{q_i}}(\alpha - \alpha_i)_+^0 \frac{\bar{q}c}{2V}$$

$$+ C_{X_{\delta_e}}\delta_e + \left(C_{X_{\delta_e}}\right)_7 \delta_e(\alpha - \alpha_7)_+^0 + \left(C_{X_{\delta_e}}\right)_{13} \delta_e(\alpha - \alpha_{13})_+^0$$

$$C_Z = C_{Z,o} + C_{Z_\alpha}\alpha + \sum_{i=1}^{K} C_{Z_{\alpha_i}}(\alpha - \alpha_i)_+ + C_{Z_q}\frac{\bar{qc}}{2V} + \sum_{i=1}^{K} C_{Z_{q_i}}(\alpha - \alpha_i)_+^0 \frac{\bar{qc}}{2V}$$

$$+ C_{Z_{\delta_e}}\delta_e + \left(C_{Z_{\delta_e}}\right)_7 \delta_e(\alpha - \alpha_7)_+^0 + \left(C_{Z_{\delta_e}}\right)_{13} \delta_e(\alpha - \alpha_{13})_+^0$$

$$C_m = C_{m,o} + C_{m_\alpha}\alpha + \sum_{i=1}^{K} C_{m_{\alpha_i}}(\alpha - \alpha_i)_+ + C_{m_q}\frac{\bar{qc}}{2V} + \sum_{i=1}^{K} C_{m_{q_i}}(\alpha - \alpha_i)_+^0 \frac{\bar{qc}}{2V}$$

$$+ C_{m_{\delta_e}}\delta_e + \left(C_{m_{\delta_e}}\right)_7 \delta_e(\alpha - \alpha_7)_+^0 + \left(C_{m_{\delta_e}}\right)_{13} \delta_e(\alpha - \alpha_{13})_+^0$$

Only two knots, α_7 and α_{13} at $\alpha = 13°$ and $\alpha = 16°$, were chosen for the elevator because of a lack of computer memory. The locations of these two knots were chosen to allow for what appeared to be the three major areas of elevator effectiveness.

After a model has been selected and parameters have been estimated, the predictive capabilities of the model must be tested. This is known as validation of the model. The method of validation used in this report is the numerical integration of the equations of motion. This method uses the estimated model and a fourth-order Runge-Kutta integration scheme. Starting with the initial conditions of the flight for which a given model was estimated, the longitudinal output variables α, q, θ, and V are computed and compared with the actual flight values for these variables. The robustness of the model can be validated by applying it to another flight with only similar initial conditions.

RESULTS AND DISCUSSION

Flight Data

A typical "flight," or experiment, for the determination of stability and control parameters consists of several "runs." Each run consists of about 3 minutes of data commencing when the airplane achieves some predetermined altitude (usually about 2000 m for a light single-engine airplane). For idle power experiments, after attaining the predetermined altitude, the throttle is closed. The airplane is then trimmed to a desired angle of attack. A control input perturbs the airplane from the trim condition with the perturbation damping out in about 4 seconds for short-period longitudinal disturbances. After the disturbance has damped, the airplane is trimmed again to some desired angle of attack and is perturbed again by a control input. In this manner, five to seven perturbations can be carried out during a single run. Each run within a flight is designated by an integer - successive runs are designated by successive integers. Each perturbation within a run is designated by a decimal point and digit appended on the run number. For example, run 7.1 indicates the first perturbation in the seventh run of a given flight; run 7.2 is the second perturbation executed in the seventh run. A run ends when the airplane approaches some predetermined minimum altitude (about 1000 m for the experiment reported herein). The air-

plane then climbs back to the initial altitude (taking about 10 minutes) and proceeds with the next run. The attitude gyros are caged (locked) between runs and uncaged at the commencement of a run.

Figure 4 presents traces for the longitudinal forces, certain lateral-motion variables, and the longitudinal control variable. The figure shows that after being perturbed from a trim angle of attack of about 13.6°, the stabilator is brought back to a position that is displaced by 1° from its trim position. While the stabilator remains in this position, the induced longitudinal oscillation does not damp out, but continues at constant amplitude until the stabilator is returned to the -5° initial condition. The time histories of the lateral-motion variables indicate that coupling between the lateral and longitudinal modes is not involved.

Figure 5 presents traces of the longitudinal-motion variables and control displacements for runs 7.1 through 7.6 and runs 8.1 through 8.5, all of which exhibit similar undamped oscillatory behavior.

Confirmation of the oscillatory region is shown in the plot of run 11 in figure 6. In this run, the airplane was trimmed to an angle of attack below that at which the undamped oscillations occurred. The stabilator deflection was increased in increments of less than 1°. The oscillation is centered around $\alpha = 14°$ and $\delta_e = -7°$.

Stabilator deflection to trim is plotted against trim angle of attack in figure 7. This figure can be used to check the actual stability of the trim conditions in the 14° to 16° angle-of-attack range. From figure 7, a loss of stabilator effectiveness to trim is indicated between $\alpha \approx 14°$ and $\alpha \approx 17.5°$.

For each run in figure 7, an uncertainty range for δ_e was calculated by averaging the 10 sample points for stabilator deflection before and the 10 sample points for stabilator deflection after the pilot noted that the airplane was trimmed. In the region above $\alpha = 14°$ and below $\alpha = 18°$, there is a very large uncertainty in the value of stabilator to trim. This uncertainty is shown by the bars about the stabilator to trim values in this region.

The lower bound on this region is further defined by runs in which the airplane is trimmed at angles of attack near 14° but pitched nose down instead of nose up. The oscillations induced in this manner do damp out. Hence, one is left with a steady-state short-period longitudinal oscillation which is easily induced from trim angles of attack in a region bounded by $\alpha = 14°$ and $\alpha = 17°$ and with stabilator deflections between -7° and -9° with the throttle set at idle power.

Comparison of Binned and Spline Analyses

Figure 8 presents the results of the stepwise regression analysis applied to three of the oscillatory flights. The circles represent linear parameters estimated from the binned analysis. Each circle is plotted according to the mean value of α for data in the bin it represents. The short-line segments in figure 8 represent the

slope of the parameters. These slopes can be identified when a second-order term such as

$$C_{Z_{\alpha^2}} = \frac{1}{2}\frac{\partial^2 C_Z}{\partial \alpha^2} = \frac{1}{2}\frac{\partial}{\partial \alpha} C_{Z_\alpha} \tag{7}$$

enters the regression equation.

As with the values of the parameters themselves, each slope for a parameter is plotted at the mean value of α for the bin in which it is identified. The ordinate value at which a slope is plotted is determined by extrapolating a line with the identified slope from the identified parameter value at the airplane trim angle of attack. (See fig. 8(a), for example.) On the plot of C_{Z_q} as a function of α in this figure, a circle is plotted at $\alpha = 11.5°$ and $C_{Z_q} = -22$. However, for the next bin, with a mean angle of attack of 12.6°, a slope is plotted. This slope (-390 rad^{-1}) is given by the value of $C_{Z_{q\alpha}}$, which is the coefficient of the $\alpha \frac{q\bar{c}}{2V}$ term identified for this bin. The value of C_{Z_q} for the data in this bin is -47 but is referred to α_o for the run which is 16.4°. Hence, the extrapolation equation for C_{Z_q} to the bin which has a mean value of $\alpha = 12.6°$ is

$$C_{Z_q}(\alpha) = -47 - 390(\alpha - \alpha_o) \tag{8}$$

where $\alpha_o = 0.2862$ radians and α is in radians. Experience has shown that such a nonzero value for a slope of a derivative indicates a region of change in the derivative value with respect to angle of attack.

Also plotted in figure 8 are the results from the application of the stepwise regression with the spline candidate model. The data are not partitioned prior to the application of the spline model. Any change in parameter values with angle of attack is noted by the entry of a knot near the region of change. Here again, the plot of C_{Z_q} as a function of α in figure 8(a) provides an example. The "staircase" or step-shaped line is the result of a spline analysis in which the stepwise regression selected zero-order splines in $(\alpha - \alpha_i)_+^0 \frac{q\bar{c}}{2V}$ with knots at $\alpha = 13.5°$ and 14.5° or a model for C_{Z_q} given (for the entire maneuver) by

$$C_{Z_q}(\alpha) = -23. - 5.5(\alpha - 0.2356)_+^0 - 5.0(\alpha - 0.2530)_+^0 \tag{9}$$

where α is in radians. An examination of the plots for each derivative in figure 8 is included in the remainder of this section.

Both the binning and spline technique show C_{Z_α} (figs. 8(a), 8(c), and 8(e)) to consist of at least two levels. For all three runs, C_{Z_α} is about -2.2 between $\alpha \approx 12°$ and $\alpha \approx 15.5°$. Above $\alpha = 15.5°$, C_{Z_α} decreases in absolute value to about -1. This corresponds to a flattening of the lift curve at about $\alpha = 15.5°$. In addition run 7.6, which contains more data from the low-angle-of-attack region, gives rise to a third level. At this level, $C_{Z_\alpha} \approx -4.5$ for $\alpha < 12°$. Overall, C_{Z_α} is strongly and consistently identified.

The derivative C_{Z_q} (figs. 8(a), 8(c), and 8(e), decreases in the region between $\alpha \approx 12°$ and $\alpha \approx 16°$ for all three runs. Run 7.6 contains an extra step in the low-angle-of-attack range. This is probably caused by a relatively large amount of data in that region, as was the case with the parameter C_{Z_α}.

The derivative C'_{m_q} (figs. 8(b), 8(d), and 8(f)) is the third strongly and consistently identified derivative. Both the binned and the spline analyses indicate positive values of C'_{m_q} between $\alpha \approx 12°$ and $\alpha \approx 17°$. Run 7.6 (fig. 8(f)) again gives the best results in the low-angle-of-attack range, where the spline technique showed that $C'_{m_q} = -13$ for $\alpha < 10.5°$.

The derivative C'_{m_α} is not identified consistently across the three runs. In run 7.1, the binned result is scattered, and the spline picks out no structure. The fact that the spline result simply averages the binned results indicates that the scatter is probably not a function of the choice of bin width and/or bin boundaries. Run 7.3 yields a bi-level value of C'_{m_α}, and the binned-value analysis indicates a drop in C'_{m_α} from -1.7 to -2.8 at $\alpha \approx 16.6°$. The spline analysis of run 7.3 shows a similar drop (but to -3.6) at $\alpha \approx 18°$. The difference in the angle of attack at which the C'_{m_α} change occurs could be explained by aliasing due to bin width and bin boundaries. Run 7.6 shows another slightly different result. The data for the low-angle-of-attack range have again resulted in better identification of C'_{m_α} at $\alpha < 12°$. The binned analysis indicates a trend from about $C'_{m_\alpha} = -1$ at $\alpha \approx 10°$ to $C'_{m_\alpha} \approx -2$ for $\alpha > 16°$. The trend is shown to support a type of double break in C'_{m_α} when analyzed by the spline technique. Each of the breaks identified by the spline model gives $C'_{m_\alpha} \approx -1$.

The derivative $C_{Z_{\delta_e}}$ is estimated consistently for $\alpha > 16°$ by both techniques as $C_{Z_{\delta_e}} = -1.2$. At lower angles of attack and in the $\alpha = 12°$ to $\alpha = 16°$ region,

the three runs yield different values. Run 7.6 again yields the result most in agreement with other data from the low-angle-of-attack region. An aliasing problem could exist with the estimation of $C_{Z_{\delta_e}}$ since, as pointed out previously, only two knots (at $\alpha = 13°$ and $\alpha = 16°$) could be chosen for δ_e.

The derivative $C'_{m_{\delta_e}}$ showed the same characteristics as $C_{Z_{\delta_e}}$. Run 7.6 presented the best low-angle-of-attack values, and all three runs yielded similar values of ≈ -1.2 for $C'_{m_{\delta_e}}$ for $\alpha > 16°$.

Interpretation of Derivatives

Because each derivative can be interpreted as a coefficient in the differential equations describing the motion of the airplane, each derivative can be interpreted as representing some characteristic behavior in that motion. The derivative C'_{m_α} represents the static margin of the airplane. A large negative increase, as seen in the analysis of runs 7.3 and 7.6, usually indicates wing stall and the resultant shift of the aerodynamic center. A positive value of C'_{m_q}, which was identified in all three runs for the region between $\alpha \approx 12°$ and $\alpha \approx 17°$, indicates positive pitch damping. Positive pitch damping indicates an unstable or divergent pitch rate in this angle of attack region. The decreasing value of $\left|C_{Z_\alpha}\right|$ can be interpreted as indicating a flattening of the lift-curve slope. This can also be interpreted as a loss in damping in $\dot{\alpha}$. The derivatives $C_{Z_{\delta_e}}$ and $C'_{m_{\delta_e}}$ indicate control effectiveness. At low angles of attack, as indicated from run 7.6, the ratio of $C'_{m_{\delta_e}}$ to $C_{Z_{\delta_e}}$ should be proportional to the moment arm for the stabilator. However, for $\alpha > 10°$, the values of $C'_{m_{\delta_e}}$ and $C_{Z_{\delta_e}}$ approach one another. These values are predicted on only a few data points overall, particularly in the oscillatory region, where the stabilator was held at $\delta_{e,o}$ for about 90 percent of the time.

Validation

After a model has been selected by an identification technique, it still must be validated in some manner. Several methods of validation are commonly used in system identification. One method compares the model derived by using one technique with that derived by using another technique. For example, the model selected by using an equation error technique can be compared with one derived by using a maximum-likelihood output error approach. Another method of validation is the testing of the predictive capabilities of the model. Given the initial conditions and forcing-function time history, the model equations can be numerically integrated, and the output variables can be compared with the actual measurement time histories of the system output variables. Another method of validation, and one which demonstrates the robustness of the model, is the combination of the initial conditions and forcing-function time histories of an experiment similar to (but not the same as) that used for the identification. Again, the output of the model should be close to the output of the actual system.

The second method, that of predictive ability, was used to validate the models derived from oscillatory data. This technique is particularly suited to the problem considered in this report, because the model was determined by minimizing the mean-square error between the measured and computed acceleration. The integrated equations of motion, however, compare output variables - total velocity V, angle of attack α, pitch rate q, and pitch angle θ. An inadequate model would fit the data to the acceleration time history, but would not, from initial conditions and a forcing-function time history, correctly predict the motion of the system.

The flight time histories for selected longitudinal variables from run 7.1, as well as the simulated time history for that run from the integrated longitudinal equations of motion with a linear aerodynamic model, are plotted in figure 9(a). Figure 9(b) shows simulated results using the spline model estimated from run 7.1. This model gives slightly better results for the angle-of-attack prediction, although it is no better than the linear model in predicting the time histories of the other three variables. Both models fail to match the total airspeed by about 10 percent at the worst points. However, the short-period oscillation in the airspeed is predicted by both the linear and nonlinear model.

As a measure of robustness of the nonlinear model, the initial conditions and forcing-function time history of run 7.3 were integrated using the nonlinear model of run 7.1. The results are presented in figure 9(c), where the simulation result is shown with the actual time history of run 7.3. Run 7.3 is a good test of the model, as it was excited with a smaller and less persistent stabilator input, and consists only of the free-oscillation response of the airplane. The model seems to be overly dependent on the forcing function, in that it predicts the first oscillation well but then allows the oscillation to damp too quickly. The model does, however, simulate the free oscillation qualitatively.

Correlations With Theoretical Models

The comparison of models estimated from flight data with those identified from wind-tunnel experiments or with those synthesized theoretically is complicated by several factors. These factors include a difference in Reynolds number, possible gust effects in flight, less repeatability of exact initial conditions in flight than in the wind tunnel, and, very importantly, an inability to separate the plunging motion of the airplane from its pitching motion in flight. The inability to separate these two motions is demonstrated in figure 10, where both $\dot{\alpha}$ (plunging) and q are plotted against time for one of the oscillatory flights. The values of $\dot{\alpha}$ for figure 10 were calculated by applying a cubic spline under tension to the angle-of-attack time history, which was indicated by the wind-vane angle-of-attack sensor on the airplane. The correlation between these two variables means that aerodynamic derivatives with respect to $\dot{\alpha}$ and q cannot be estimated separately, but rather some combination must be estimated. The actual combinations that are estimated are derived for the pitching-moment derivatives in the appendix. Within the framework of the above difficulties, the models estimated from the flight data were compared with two theoretical models. The first type of model was developed by Phillips (ref. 1). The model demonstrates that the dynamic effect of $\dot{\alpha}$ near $C_{L,max}$ of the wing and the associated hysteresis in the lift curve can produce an oscillatory longitudinal motion. Hence, this first model deals principally with the effect of the wing. The second model considered here places the cause of the oscillation mainly on the tail. In this second model, when $C_{m_q} > 0$ in a small α region, a total loss of damping in pitch is indicated. Hence, a longitudinal oscillation develops to a limit cycle.

Both models are considered individually. The Phillips models are of interest in light of the results of Winkelmann (ref. 9) and the new wind-tunnel results of Newsom, Satran, and Johnson (ref. 4). These results indicate either hysteresis or uncertainty in the lift-curve slope in certain angle-of-attack regions. This section of the present report is an investigation of existence of hysteretic behavior in the actual flight data.

Phillips models.- To apply the stepwise regression for the purpose of estimating a model structure similar to the Phillips models, the set of candidate model variables was modified to include the variables $\sqrt{\dot{\alpha}}$ and $\sqrt{\dot{\alpha}}\,\alpha$. The $\sqrt{\dot{\alpha}}$ and $\sqrt{\dot{\alpha}}\,\alpha$ terms were restricted to $\dot{\alpha} > 0$, in that it was only for these positive values of $\dot{\alpha}$ that the augmentation of the lift curve is postulated. The values of $\dot{\alpha} < 0$ are ignored by the program when creating the data string for the $\sqrt{\dot{\alpha}}$ and $\sqrt{\dot{\alpha}}\,\alpha$ terms. Of the 11 oscillatory runs that were analyzed, only 3 yielded a C_Z parameter proportional to $\sqrt{\dot{\alpha}}$. In each case, the identified parameter was $C_{Z_{\sqrt{\dot{\alpha}}\,\alpha}}$ and $C_{Z_{\sqrt{\dot{\alpha}}}}$ was zero. A typical value for $C_{Z_{\sqrt{\dot{\alpha}}\,\alpha}}$ was -12.5 ± 2.0. This value of $C_{Z_{\sqrt{\dot{\alpha}}\,\alpha}}$ implies an increase in $C_{L,max}$ as a linear function of the difference between flight reference angle of attack and stall angle of attack.

A second feature of the Phillips models was hysteresis in the lift curve. To identify possible hysteresis from the flight data, 2 bins were created for each of the 11 runs. All data corresponding to $\dot{\alpha} > 0$ were put in the first bin. The other bin contained data corresponding to $\dot{\alpha} < 0$. The stepwise regression was applied to each bin for each of the 11 runs. In 10 of the 11 runs, the bin for $\dot{\alpha} > 0$ yielded a greater lift-curve slope than the bin for $\dot{\alpha} < 0$. The results for lift-curve slope are given in figure 11. It is clear from the figure that for all runs except 7.1, the lift-curve slope is greater for $\dot{\alpha} > 0$ than for $\dot{\alpha} < 0$. For run 7.1, the two slopes are the same. The dashed lines in figure 11 depict higher-order derivative information (e.g., $C_{Z_{\alpha^2}}$, $C_{Z_{\alpha^3}}$, etc.) extracted by the stepwise regression. When this same technique was applied to data from maneuvers by the same airplane trimmed at lower angles of attack ($\alpha = 4°$ to $\alpha = 5°$), there was no significant difference in lift-curve slope.

Finally, approximate values of C_L, calculated using

$$C_L \approx -C_Z \approx -C_{Z_o} - C_{Z_\alpha}(\alpha - \alpha_o) + (\text{higher-order term where identified}) \qquad (10)$$

are plotted in figure 12 for models from the three representative runs - 7.1, 7.3, and 7.6. Again, the differences in lift for $\dot{\alpha} > 0$ compared with $\dot{\alpha} < 0$ for α in the oscillatory region are evident. When the maneuvers initiated from lower angles of attack were analyzed using a similar binning as a function of $\dot{\alpha}$, no differences in lift curve were evident.

In summary, differences in lift-curve value and lift-curve slope appear in data from the longitudinal maneuvers initiated from angles of attack near 16°, but not in data from similar maneuvers initiated from lower trim angles of attack ($\alpha = 4°$ to 5°). Moreover, in the region in which the differences exist, the lift-curve slope and lift-curve value are greater for increasing angle of attack ($\alpha > 0$). Such a result agrees with the Winkelmann (ref. 9) results for a similar wing in a wind-tunnel test.

Van der Pol model.- In reference 2, Thomas and Collingbourne describe a deep-stall limit-cycle condition by a Van der Pol-type differential equation. The Van der Pol equation has the general form

$$\ddot{z}(t) - \varepsilon[1 - z^2(t)]\,\dot{z}(t) + z(t) = 0 \tag{11}$$

The solution to equation (11) is a limit cycle because of the change in the sign of the damping coefficient $\varepsilon[1 - z^2(t)]$ that occurs whenever $z(t)$ traverses the values ± 1. For application to the airplane problem, the perturbation $\Delta\alpha$, in angle of attack from α_o, can be substituted for $z(t)$ in equation (11) to yield

$$\Delta\ddot{\alpha} = \theta_2\,\Delta\dot{\alpha} + \theta_3\,\Delta\dot{\alpha}(\Delta\alpha)^2 + \theta_1\,\Delta\alpha \tag{12}$$

Equation (12) is in a form amenable to solution for $\hat{\theta}_1$, $\hat{\theta}_2$, and $\hat{\theta}_3$ by the stepwise regression program with the independent variables $\Delta\dot{\alpha}$ and $\Delta\alpha$. Then the frequency of oscillation of the system can be estimated by

$$\omega_{osc} = \sqrt{-\hat{\theta}_1}$$

Also, $(\Delta\alpha)_{crit}$, the $\Delta\alpha$ value at which the damping of the motion changes sign, is given by

$$(\Delta\alpha)_{crit} = \sqrt{-\frac{\hat{\theta}_2}{\hat{\theta}_3}}$$

Applying the stepwise regression to the data from run 7.3 yields $\hat{\theta}_1 = -7.4$, $\hat{\theta}_2 = -0.52$, and $\hat{\theta}_3 = 183$. These three values are typical of the other oscillatory runs. For these values of $\hat{\theta}_1$, $\hat{\theta}_2$, and $\hat{\theta}_3$, $\omega_{sc} = 2.7$ rad/sec, and $(\Delta\alpha)_{crit} = \pm 3.1°$. These values are corroborated by the flight data. The interpretation of the Van der Pol results is that the $\Delta\dot{\alpha}$ term provides no damping and in fact tends to increase $|\alpha - \alpha_o|$ to 3.1°, when the coefficient of $\Delta\dot{\alpha}$ changes sign and provides damping.

Another derivation of the Van der Pol coeffic nts comes from extracting pitching-moment derivatives. If the pitching-moment equation is written as

$$I_Y\dot{q} = \frac{1}{2}\rho V^2 S\bar{c}\left[C'_{m_\alpha}\,\Delta\alpha + C'_{m_q}\,\frac{q\bar{c}}{2V} \quad C'_{m_{\alpha^2 q}}(\Delta\alpha)^2\,\frac{q\bar{c}}{2V}\right] \tag{13}$$

and if $\dot{\alpha} \equiv q$ for a single degree of freedom, then equation (13) becomes

$$\ddot{\Delta\alpha} = \frac{\rho V^2 S\bar{c}}{2I_Y} C'_{n_q} \frac{\dot{\Delta\alpha}\,\bar{c}}{2V} + \frac{\rho V^2 S\bar{c}}{2I_Y} C'_{m_{\alpha^2 q}} (\Delta\alpha)^2 \frac{\dot{\Delta\alpha}\,\bar{c}}{2V} + \frac{\rho V^2 S\bar{c}}{2I_Y} C'_{m_\alpha} \Delta\alpha \qquad (14)$$

Substituting values from run 7.1, then $\omega_{osc} = 2.7$ rad/sec and $(\Delta\alpha)_{crit} = \pm 3.0°$, which is again in agreement with the flight data. To validate the single-degree-of-freedom Van der Pol model, the model equation was integrated numerically using a fourth-order Runge-Kutta integration scheme. A phase-plane plot of the results of such an integration using the Van der Pol model from run 7.3 and realistic initial conditions of $\Delta\alpha = 0$ and $q = -0.16$ rad/sec is presented in figure 13(a). In all parts of figure 13, the sense of increasing time is clockwise. This model reaches its limit cycle trajectory in about two complete cycles. However, in figure 13(b), a phase-plane plot of the actual flight data indicates that a much more rapid transition to the limit cycle trajectory (in about one-fourth of a cycle) should be expected. Moreover, $(\Delta\alpha)_{crit}$ corresponds to the maximum deviation in α. In order to predict this maximum deviation, the damping should change sign at a smaller value of $\Delta\alpha$. In summary, the Van der Pol single-degree-of-freedom equation correctly predicts the qualitative behavior of the motion but fails to predict correctly the variation in angle of attack.

For completeness, two additional cases were numerically integrated, and their phase-plane trajectories were plotted. In figure 13(c), the Van der Pol model from run 7.3 is integrated from initial conditions $\Delta\alpha = 0$ and $q = -0.45$ rad/sec. These conditions lead to the same limit cycle trajectory as did the conditions that yielded the results shown in figure 13(a). Finally, a linear harmonic oscillator estimated from the equation $\ddot{\alpha} = \theta_1 \alpha$ was integrated, and the resulting phase-plane trajectory was plotted in figure 13(d). Though it satisfies the range requirement for α, the harmonic oscillator model fails to satisfy the range requirement for q and, most importantly, fails to have the qualitative property of converging from any given initial condition to the same limit cycle trajectory.

CONCLUSIONS

Several examples of short period longitudinal oscillatory flight at high values of lift coefficient have been analyzed. The data were obtained by a light single-engine research airplane with outboard leading-edge modifications for operation at high angles of attack. A stepwise regression was applied to the flight data to determine aerodynamic force and moment model structure and parameter values. Two separate applications of the stepwise regression were made, each with different forms of the candidate models. In one application, the candidate model set was comprised of spline basis functions with knots at 0.5° increments in angle of attack. The other application consisted of applying the stepwise regression with polynomial candidate model terms to the data after that data had been partitioned into bins as a function of angle of attack. An analysis of the results, including a comparison with theory, indicates the following:

1. The change in pitching moment with respect to pitch rate C'_{m_q} is definitely positive for the angle-of-attack range over which the oscillations occur. There is a flattening of the lift curve in the oscillatory region. The values of the change in pitching moment with respect to angle of attack C'_{m_α}, though not consistent, imply the possibility of a stall in the oscillatory region.

2. Both techniques (polynomial on a partitioned data set and spline) give similar results.

3. The models simulate the oscillatory behavior qualitatively but provide too much damping.

4. Analysis of data partitioned for positive and negative rates of change of angle of attack gives strong support for the existence of a hysteresis loop in the lift curve for the angle-of-attack range covered by the oscillatory motion.

5. A one-degree-of-freedom Van der Pol model can simulate the general phase-plane behavior of the motion but does not properly limit the range of angle of attack.

Langley Research Center
National Aeronautics and Space Administration
Hampton, VA 23665
November 30, 1982

APPENDIX

EQUATIONS OF MOTION

The following equations of motion are given in this appendix.

$$\dot{u} = -qw + rv - g \sin\theta + \frac{\rho V^2 S}{2m} C_X$$

$$\dot{v} = -ru + pw + g \cos\theta \sin\phi + \frac{\rho V^2 S}{2m} C_Y$$

$$\dot{w} = -pv + qu + g \cos\theta \cos\phi + \frac{\rho V^2 S}{2m} C_Z$$

$$\dot{p} = qr\left(\frac{I_Y - I_Z}{I_X}\right) + \frac{I_{XZ}}{I_X}(pq + \dot{r}) + \frac{\rho V^2 Sb}{2I_X} C_l$$

$$\dot{q} = pr\left(\frac{I_Z - I_X}{I_Y}\right) + \frac{I_{XZ}}{I_Y}(r^2 - p^2) + \frac{\rho V^2 S\bar{c}}{2I_Y} C_m'$$

$$\dot{r} = pq\left(\frac{I_X - I_Y}{I_Z}\right) + \frac{I_{XZ}}{I_Z}(\dot{p} - qr) + \frac{\rho V^2 Sb}{2I_Z} C_n$$

$$\dot{\theta} = q \cos\phi - r \sin\phi$$

$$\dot{\phi} = p + (q \sin\phi + r \cos\phi) \tan\theta$$

$$V = \sqrt{u^2 + v^2 + w^2}$$

$$\alpha = \tan^{-1}\frac{w}{u} \qquad \dot{\alpha} \approx \frac{\dot{w}}{u}$$

$$\beta = \sin^{-1}\frac{v}{V} \qquad \dot{\beta} \approx \frac{\dot{v}}{V}$$

where

$$C_Z = C_{Z,o} + C_{Z_\alpha}(\alpha - \alpha_o) + C_{Z_q}\frac{q\bar{c}}{2V} + C_{Z_{\delta_e}}(\delta_e - \delta_{e,o}) + C_{Z_{q\alpha}}(\alpha - \alpha_o)\frac{q\bar{c}}{2V}$$
$$+ C_{Z_{\alpha^2}}(\alpha - \alpha_o)^2 + C_{Z_{\delta_e\alpha}}(\alpha - \alpha_o)(\delta_e - \delta_{e,o}) + C_{Z_{\beta^2}}(\beta - \beta_o)^2$$
$$+ C_{Z_{\beta^2\alpha}}(\beta - \beta_o)^2(\alpha - \alpha_o) + C_{Z_{\alpha^3}}(\alpha - \alpha_o)^3 + C_{Z_{\alpha^4}}(\alpha - \alpha_o)^4$$
$$+ C_{Z_{\alpha^5}}(\alpha - \alpha_o)^5 + C_{Z_{\alpha^6}}(\alpha - \alpha_o)^6 + C_{Z_{\alpha^7}}(\alpha - \alpha_o)^7 + C_{Z_{\alpha^8}}(\alpha - \alpha_o)^8$$

$$C'_m = C'_{m,o} + C'_{m_\alpha}(\alpha - \alpha_o) + C'_{m_q}\frac{q\bar{c}}{2V} + C'_{m_{\delta_e}}(\delta_e - \delta_{e,o}) + C'_{m_{q\alpha}}(\alpha - \alpha_o)\frac{q\bar{c}}{2V}$$
$$+ C'_{m_{\alpha^2}}(\alpha - \alpha_o)^2 + C'_{m_{\delta_e\alpha}}(\delta_e - \delta_{e,o})(\alpha - \alpha_o) + C'_{m_{\beta^2\alpha}}(\beta - \beta_o)^2(\alpha - \alpha_o)$$
$$+ C'_{m_{\beta^2}}(\beta - \beta_o)^2 + C'_{m_{\alpha^3}}(\alpha - \alpha_o)^3 + C'_{m_{\alpha^4}}(\alpha - \alpha_o)^4 + C'_{m_{\alpha^5}}(\alpha - \alpha_o)^5$$
$$+ C'_{m_{\alpha^6}}(\alpha - \alpha_o)^6 + C'_{m_{\alpha^7}}(\alpha - \alpha_o)^7 + C'_{m_{\alpha^8}}(\alpha - \alpha_o)^8$$

where

$$C'_{m,o} = C_{m,o} + C_{m_\alpha^\bullet}\left(\frac{\rho S\bar{c}}{4m} C_{Z,o} + \frac{q\bar{c}}{2V^2}\cos\theta_o\right)$$

$$C'_{m_\alpha} = C_{m_\alpha} + \frac{\rho S\bar{c}}{4m} C_{m_\alpha^\bullet} C_{Z_\alpha}$$

$$C'_{m_q} = C_{m_q} + C_{m_\alpha^\bullet}\left(1 + \frac{\rho S\bar{c}}{4m} C_{Z_q}\right)$$

$$C'_{m_{\delta_e}} = C_{m_{\delta_e}} + \frac{\rho S\bar{c}}{4m} C_{m_\alpha^\bullet} C_{Z_{\delta_e}}$$

$$C'_{m_{q\alpha}} = C_{m_{q\alpha}} + C_{m_\alpha^\bullet}\frac{\rho S\bar{c}}{4m} C_{Z_{q\alpha}}$$

$$C'_{m_{\alpha^2}} = C_{m_{\alpha^2}} + C_{m_{\dot{\alpha}}} \frac{\rho S \bar{c}}{4m} C_{Z_{\alpha^2}}$$

$$C'_{m_{\delta_e \alpha}} = C_{m_{\delta_e \alpha}} + C_{m_{\dot{\alpha}}} \frac{\rho S \bar{c}}{4m} C_{Z_{\delta_e \alpha}}$$

$$C'_{m_{\beta^2 \alpha}} = C_{m_{\beta^2 \alpha}} + C_{m_{\dot{\alpha}}} \frac{\rho S \bar{c}}{4m} C_{Z_{\beta^2 \alpha}}$$

$$C'_{m_{\beta^2}} = C_{m_{\beta^2}} + C_{m_{\dot{\alpha}}} \frac{\rho S \bar{c}}{4m} C_{Z_{\beta^2}}$$

$$C'_{m_{\alpha i}} = C_{m_{\alpha i}} + C_{m_{\dot{\alpha}}} \frac{\rho S \bar{c}}{4m} C_{Z_{\alpha i}}$$

Assuming steady-state ($v_o = p_o = q_o = r_o = \phi_o = 0$) initial flight conditions, the longitudinal equations become

$$\dot{u} = -qw - g \sin \theta + \frac{\rho V^2 S}{2m} C_X$$

$$\dot{w} = qu + g \cos \theta + \frac{\rho V^2 S}{2m} C_Z$$

$$\dot{q} = \frac{\rho V^2 S \bar{c}}{2I_Y} C'_m$$

$$\dot{\theta} = q$$

and the longitudinal output can be written as

$$a_X = \frac{1}{g}(\dot{u} + qw + g \sin \theta)$$

$$a_Z = \frac{1}{g}(\dot{w} - qu - g \cos \theta)$$

and for the equation error form, the aerodynamic coefficients can be written as

$$\frac{2qm}{\rho V^2 S} a_X = C_X$$

$$\frac{2qm}{\rho V^2 S} a_Z = C_Z$$

$$\frac{2I_Y}{\rho V^2 S\bar{c}} \dot{q} = C'_m$$

REFERENCES

1. Phillips, William H.: Simulation Study of the Oscillatory Longitudinal Motion of an Airplane at the Stall. NASA TP-1242, 1978.

2. Thomas, H. H. B. M.; and Collingbourne, Joan: Longitudinal Motions of Aircraft Involving High Angles of Attack. R. & M. No. 3753, British A.R.C., 1974.

3. Montgomery, Raymond C.; and Moul, Martin T.: Analysis of Deep-Stall Characteristics of T-Tailed Aircraft Configurations and Some Recovery Procedures. J. Aircr., vol. 3, no. 6, Nov.-Dec. 1966, pp. 562-566.

4. Newsom, William A., Jr.; Satran, Dale R.; and Johnson, Joseph L., Jr.: Effects of Wing-Leading-Edge Modifications on a Full-Scale, Low-Wing General Aviation Airplane - Wind-Tunnel Investigation of High-Angle-of-Attack Aerodynamic Characteristics. NASA TP-2011, 1982.

5. Mulder, J. A.; and den Hollander, J. G.: Status of Dynamic Flight Test Technology - Model Identification for Flight Simulation. SAE Tech. Paper Series 810597, Apr. 1981.

6. Zadeh, L. A.: From Circuit Theory to System Theory. Proc. IRE, vol. 50, no. 5, May 1962, pp. 856-865.

7. Klein, Vladislav; Batterson, James G.; and Murphy, Patrick C.: Determination of Airplane Model Structure From Flight Data by Using Modified Stepwise Regression. NASA TP-1916, 1981.

8. Batterson, James G.: Estimation of Airplane Stability and Control Derivatives From Large Amplitude Longitudinal Maneuvers. NASA TM-83185, 1981.

9. Winkelmann, Allen E.: An Experimental Study of Separated Flow on a Finite Wing. AIAA-81-1882, Aug. 1981.

TABLE 1.- CANDIDATE MODEL VARIABLES

α	α^2	β^2	α^3
q	αq	$\beta^2\alpha$	α^4
δ_e	$\alpha\delta_e$		α^5
			α^6
			α^7
			α^8

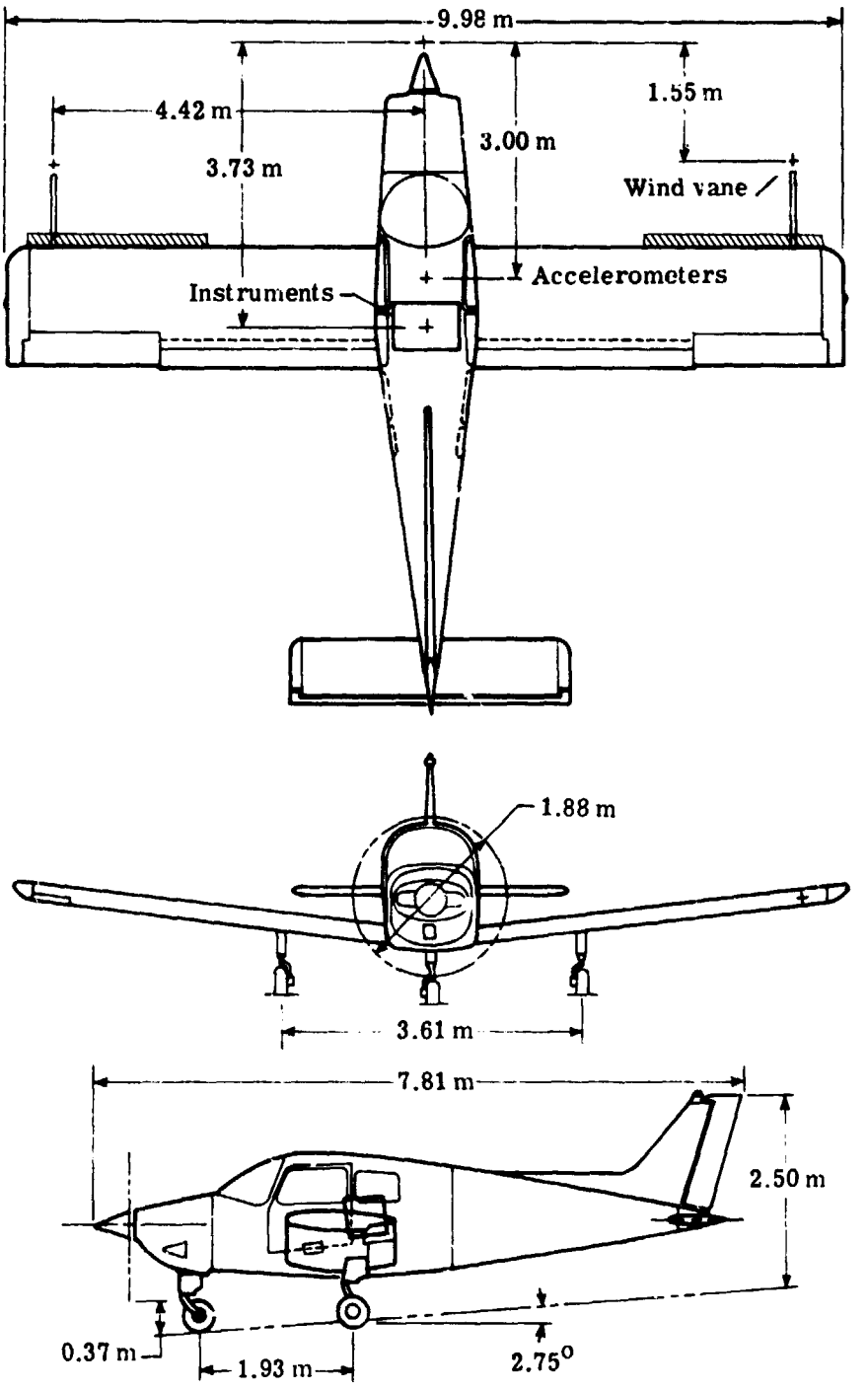

Figure 1.- Three-view drawing of test airplane showing outboard leading-edge modifications (not to scale) on top view.

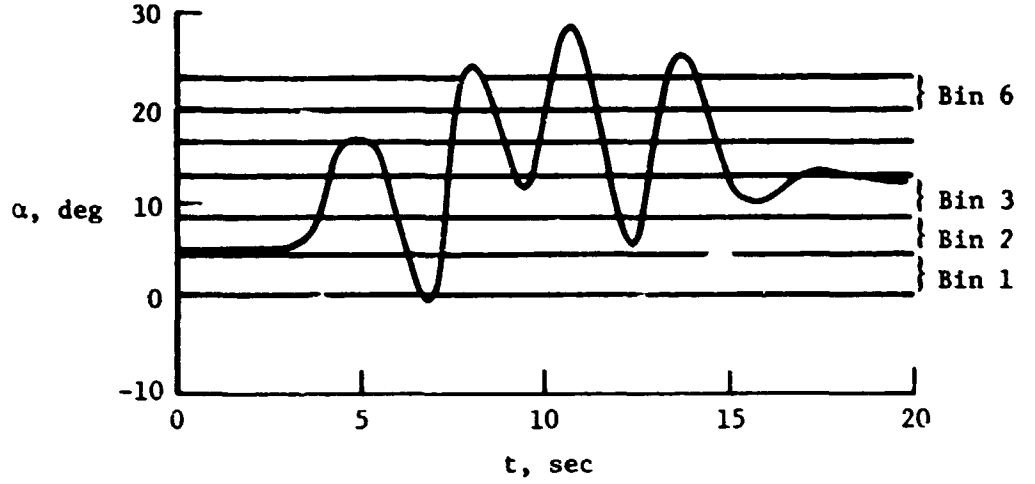

Figure 2.- Data partitioning for a large-amplitude longitudinal maneuver.

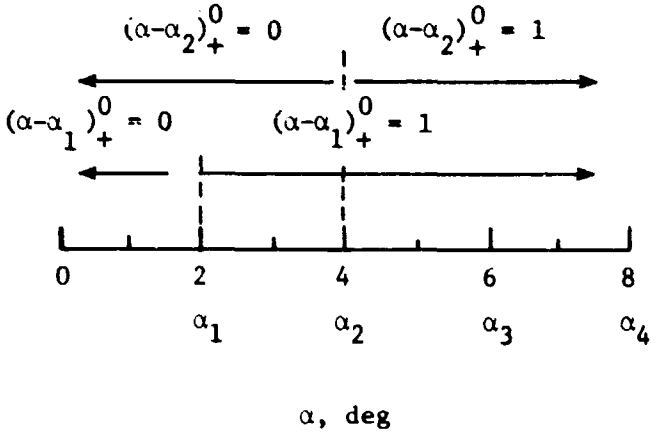

Figure 3.- Regions of support for spline basis functions.

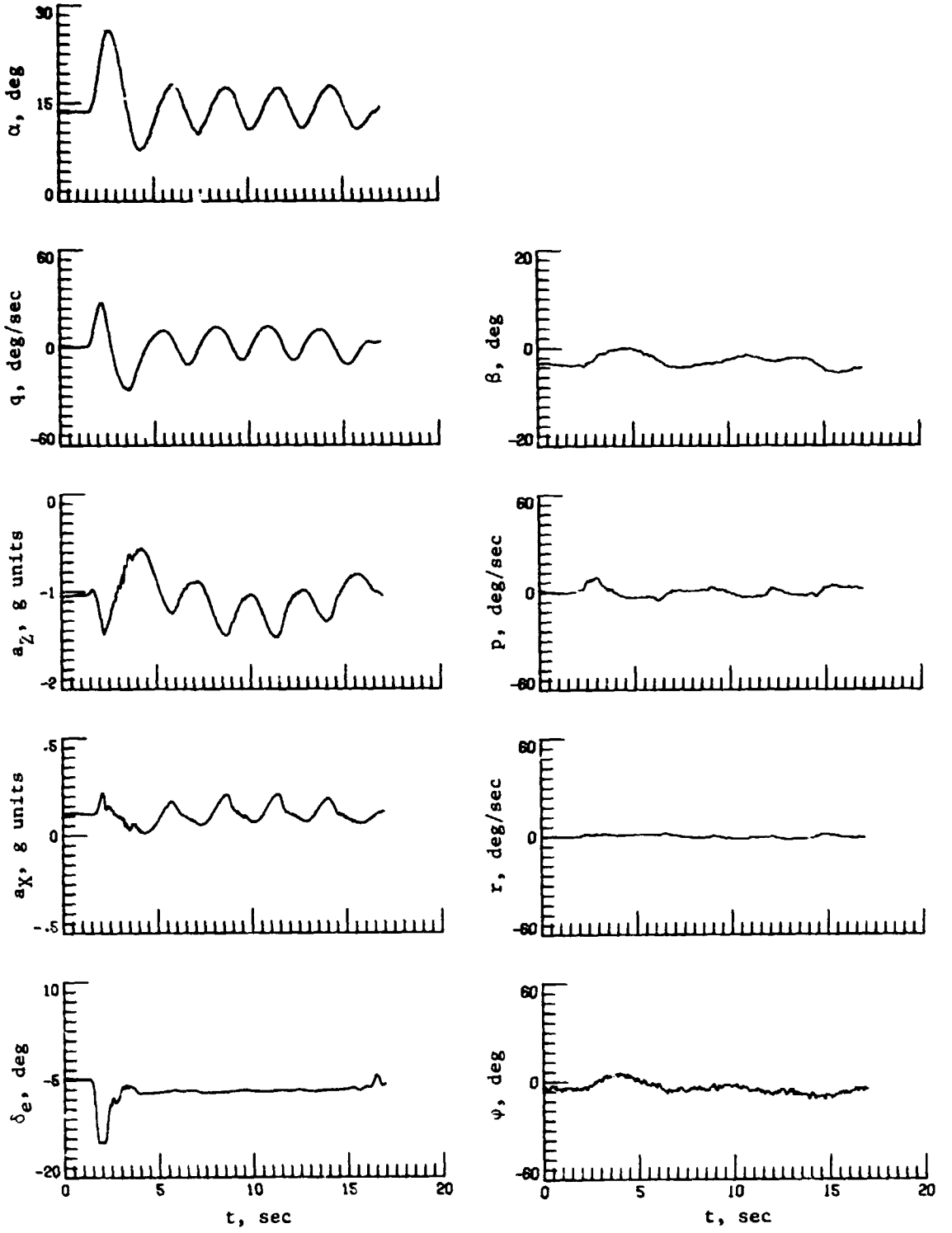

Figure 4.- Time histories of selected longitudinal and lateral variables for run 5.4.

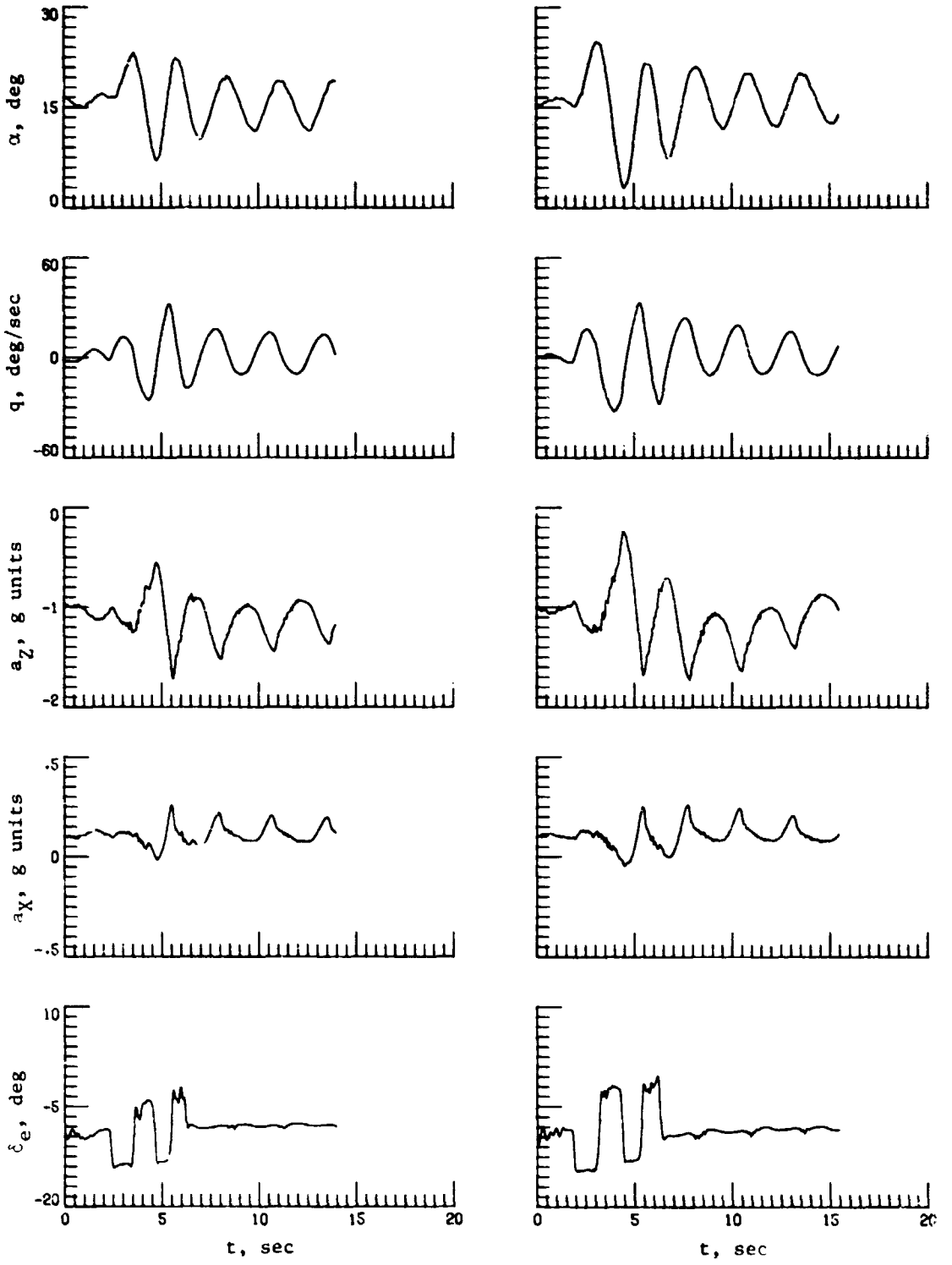

(a) Run 7.1.

(b) Run 7.2.

Figure 5.- Time histories of selected longitudinal variables for oscillatory flights.

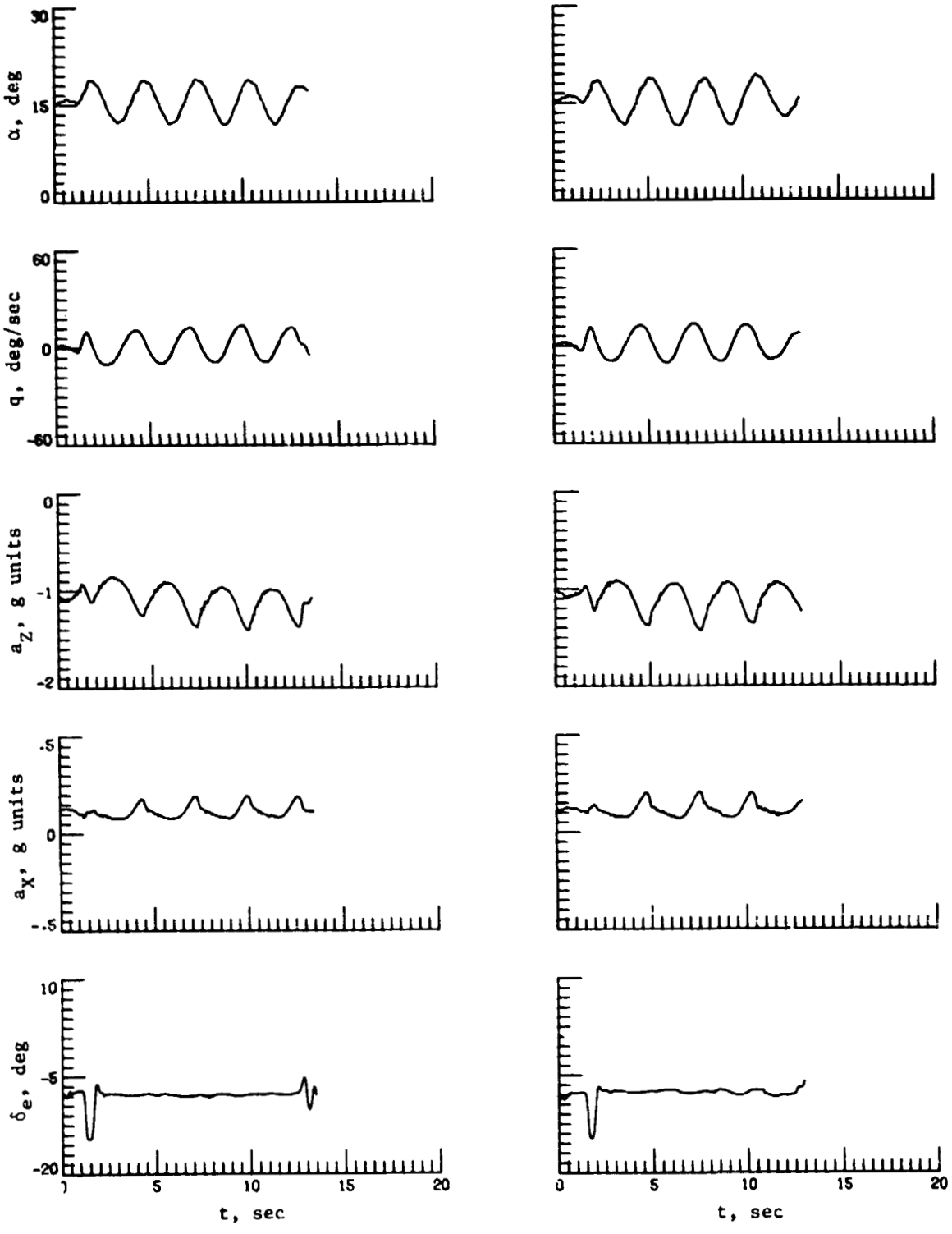

(c) Run 7.3.

(d) Run 7.4.

Figure 5.- Continued.

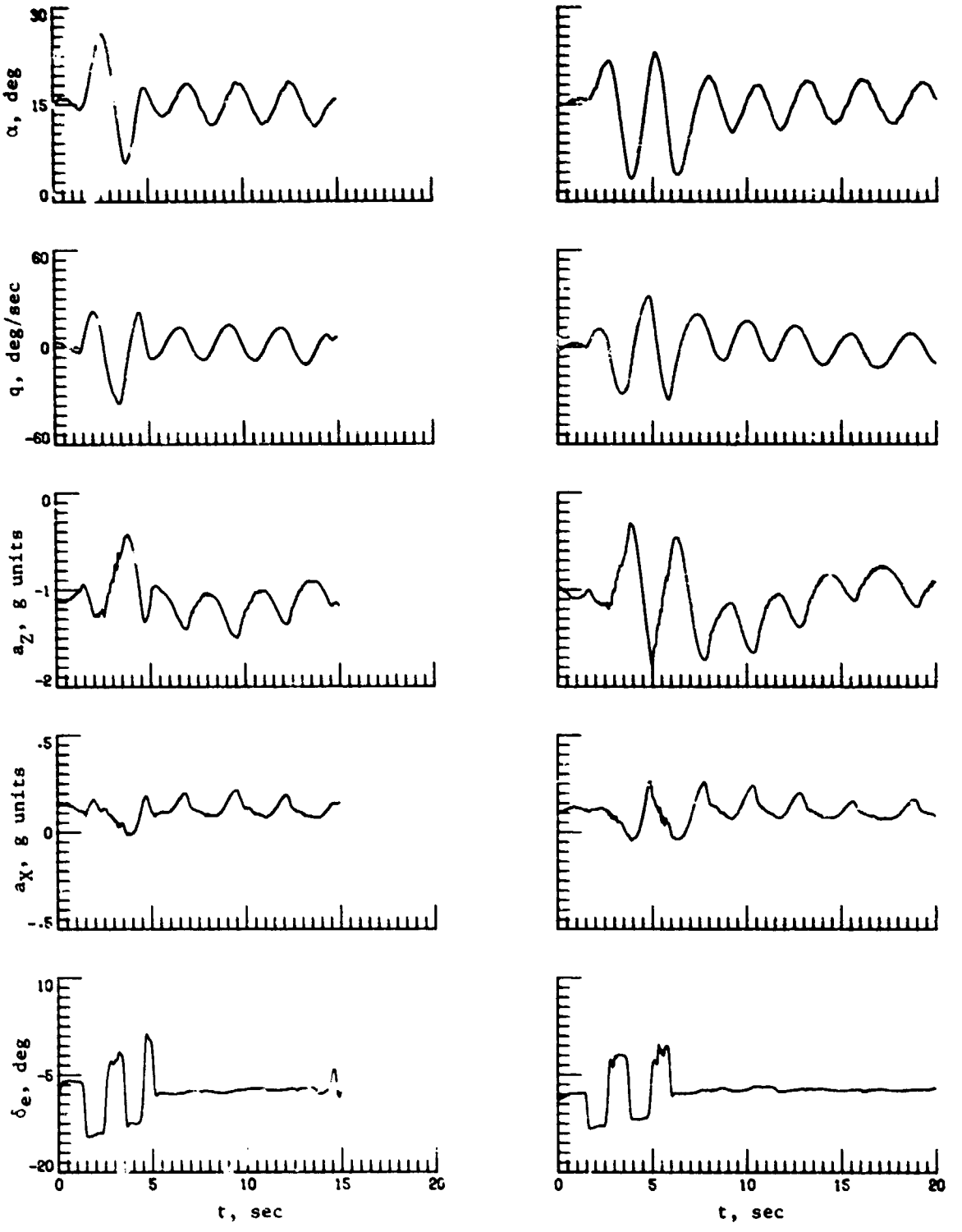

(e) Run 7.5.

(f) Run 7.6.

Figure 5.- Continued.

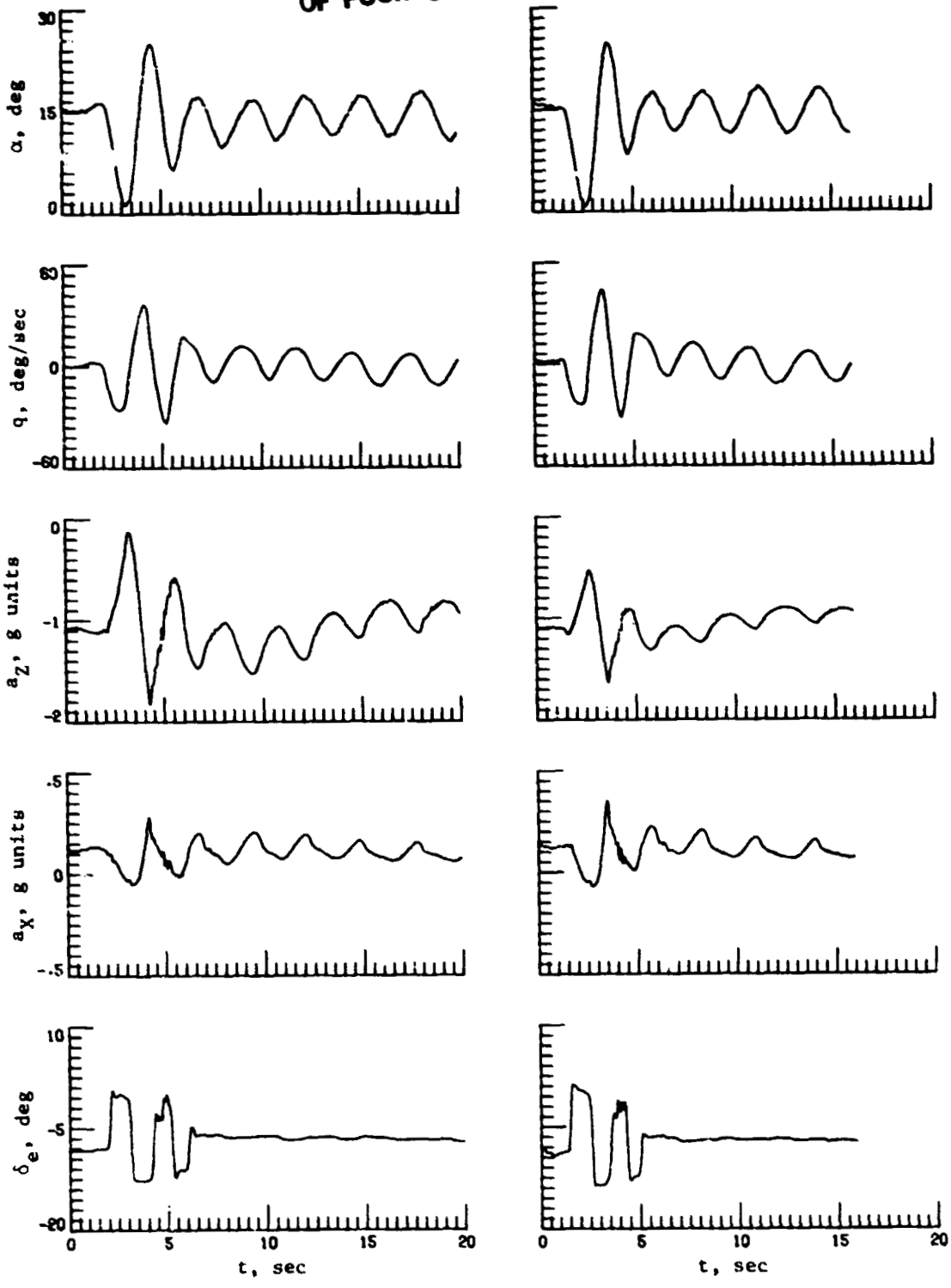

(g) Run 8.1.

(h) Run 8.2.

Figure 5.- Continued.

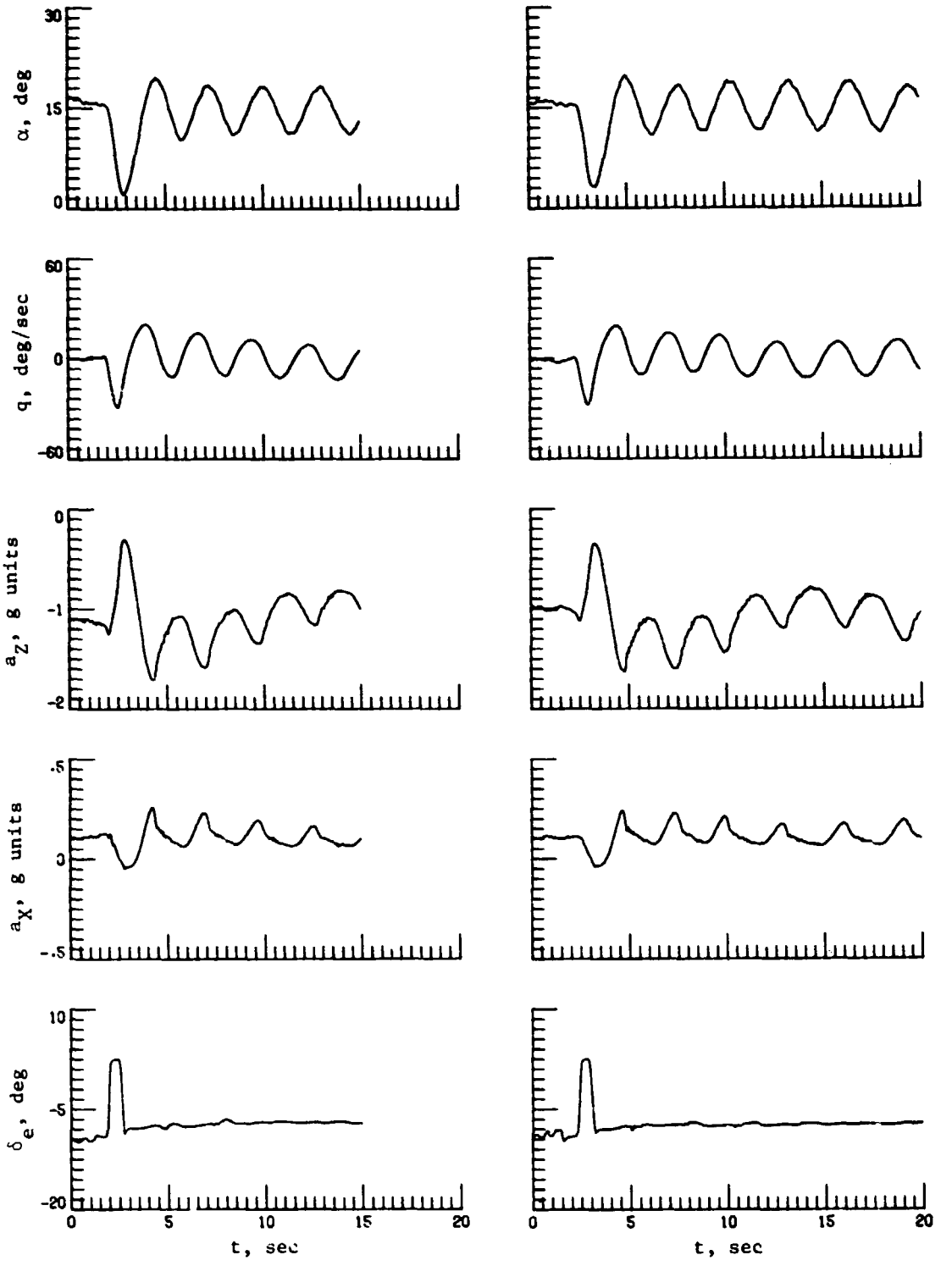

(i) Run 8.3.

(j) Run 8.4.

Figure 5.- Continued.

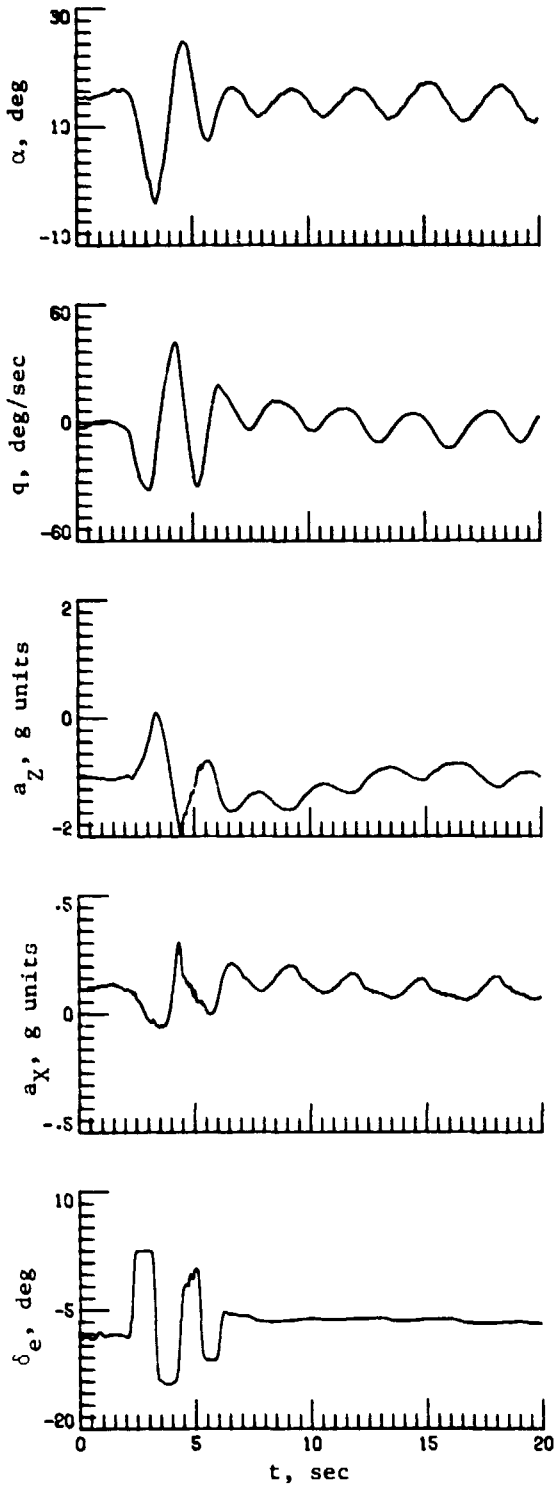

(k) Run 8.5.

Figure 5.- Concluded.

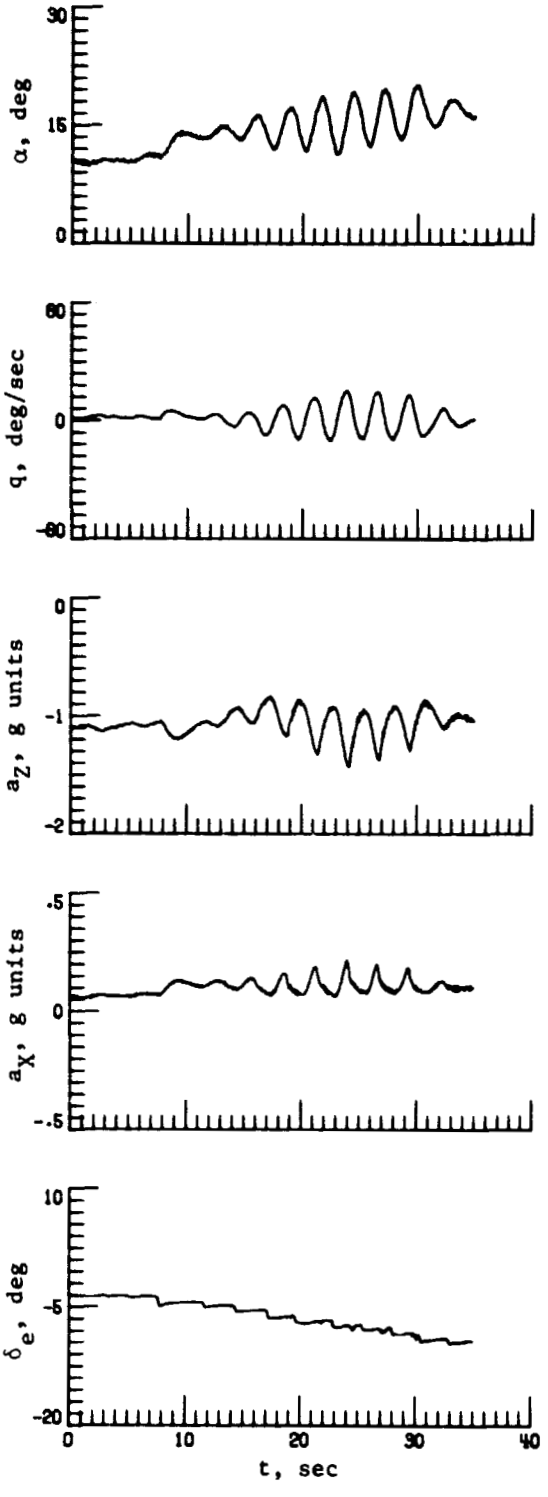

Figure 6.- Time history for deceleration maneuver in which stabilator was brought up to full stop to show development of oscillations (run 11).

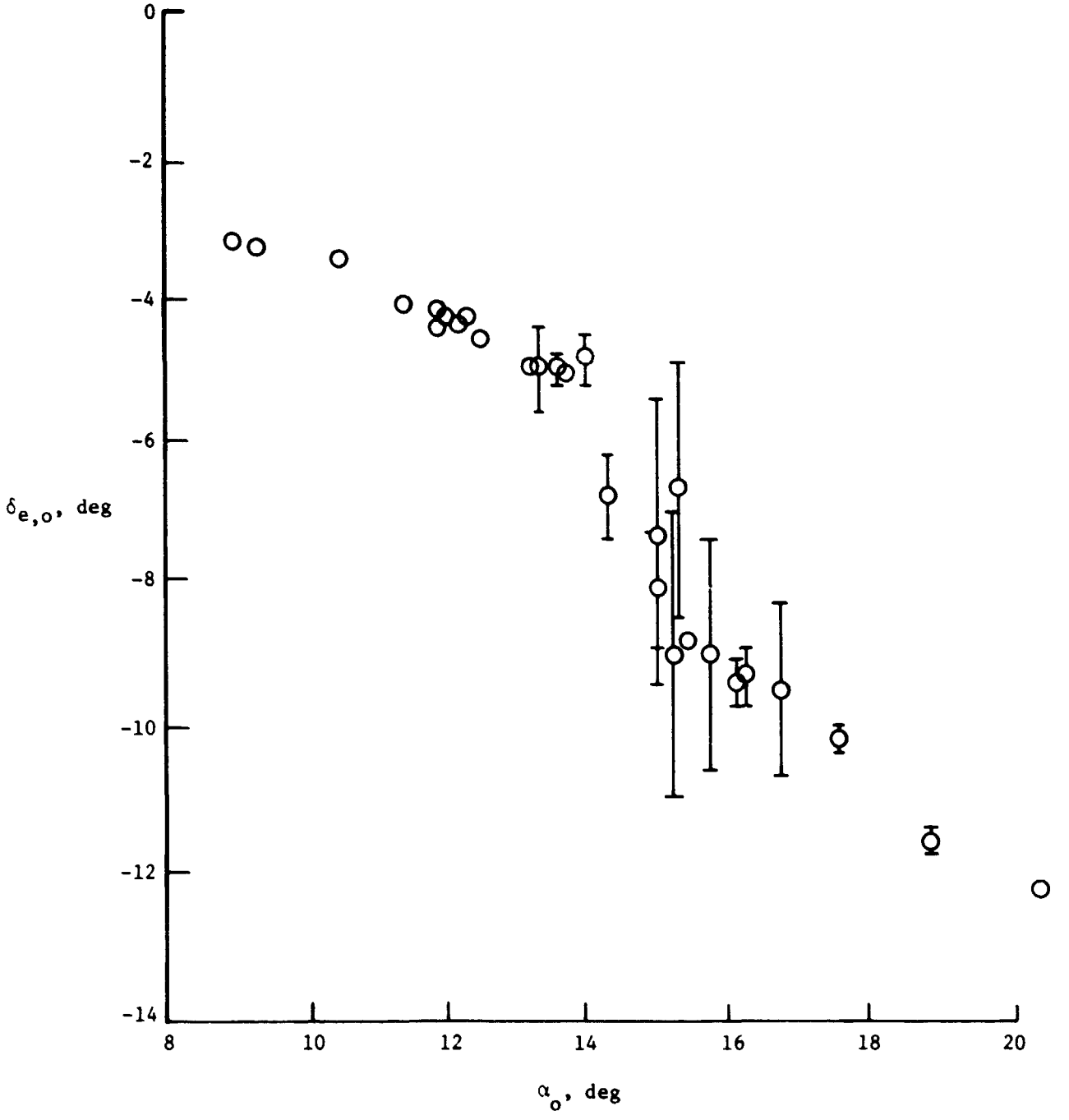

Figure 7.- Stabilator trim deflection plotted against angle-of-attack trim curve showing uncertainty in stabilator trim deflection for α_o between 14° and 18°.

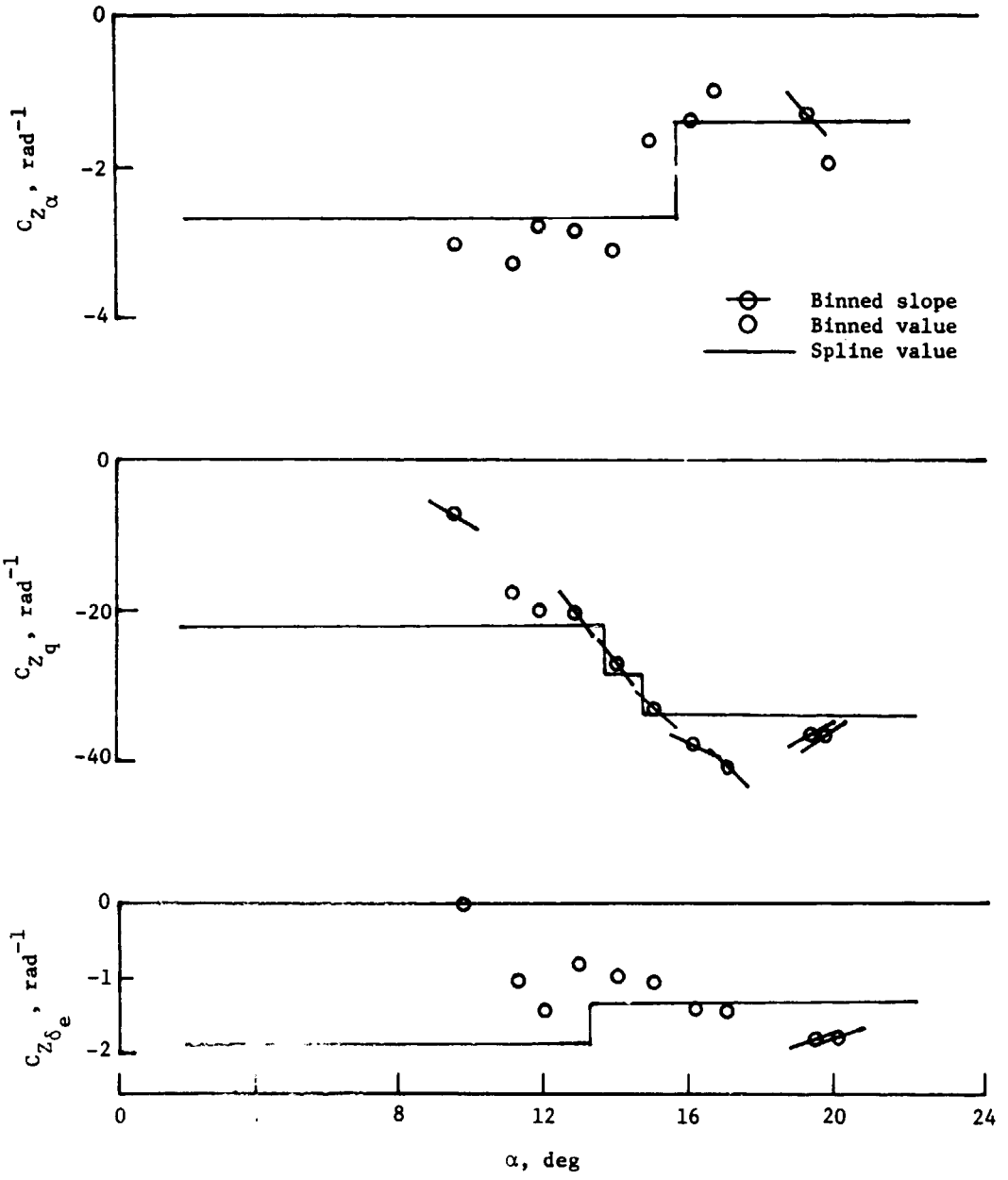

(a) Z-force coefficients for run 7.1.

Figure 8.- Aerodynamic derivatives estimated using stepwise regression with polynomial model on partitioned data and spline modes.

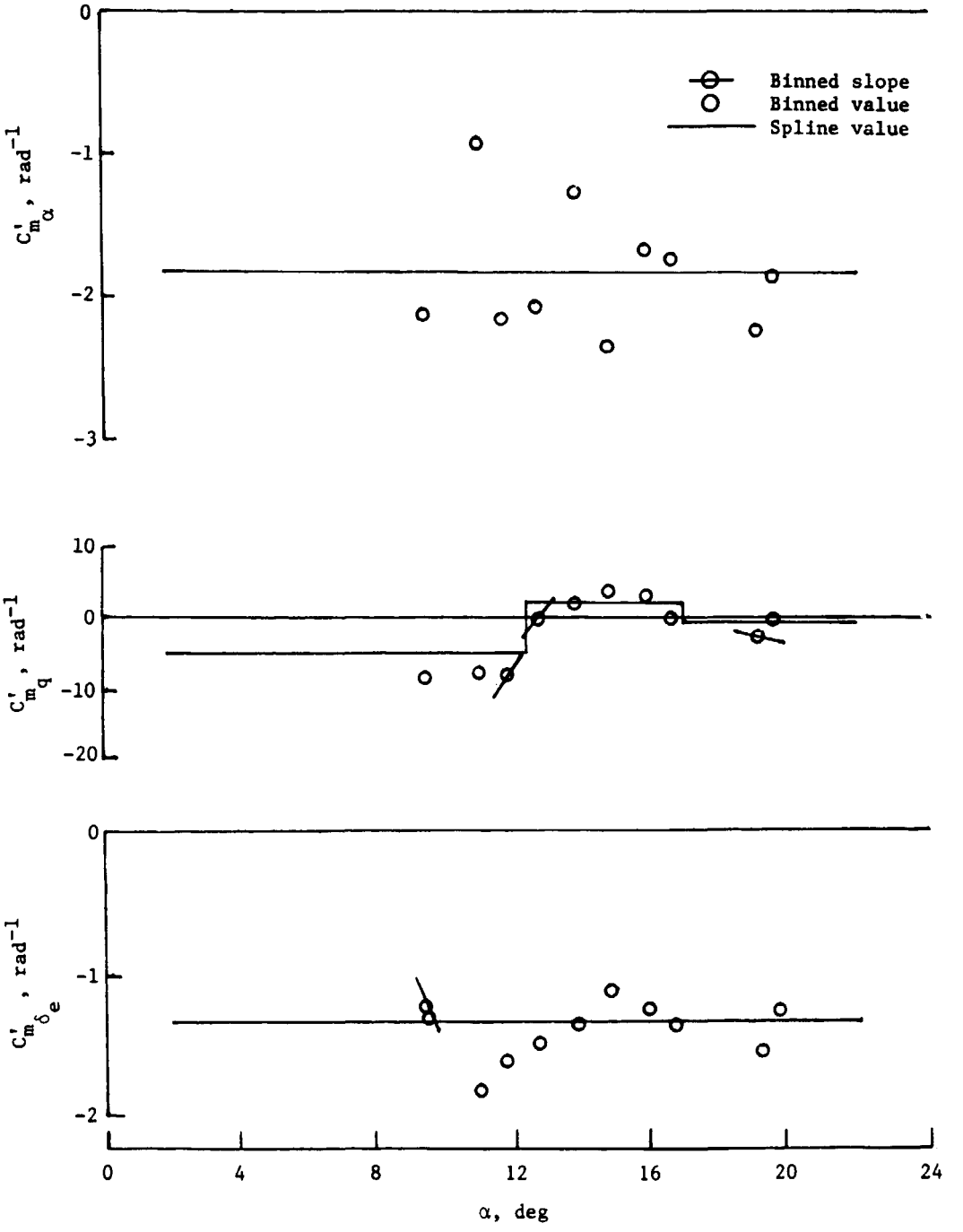

(b) Pitching-moment coefficients for run 7.1.

Figure 8.- Continued.

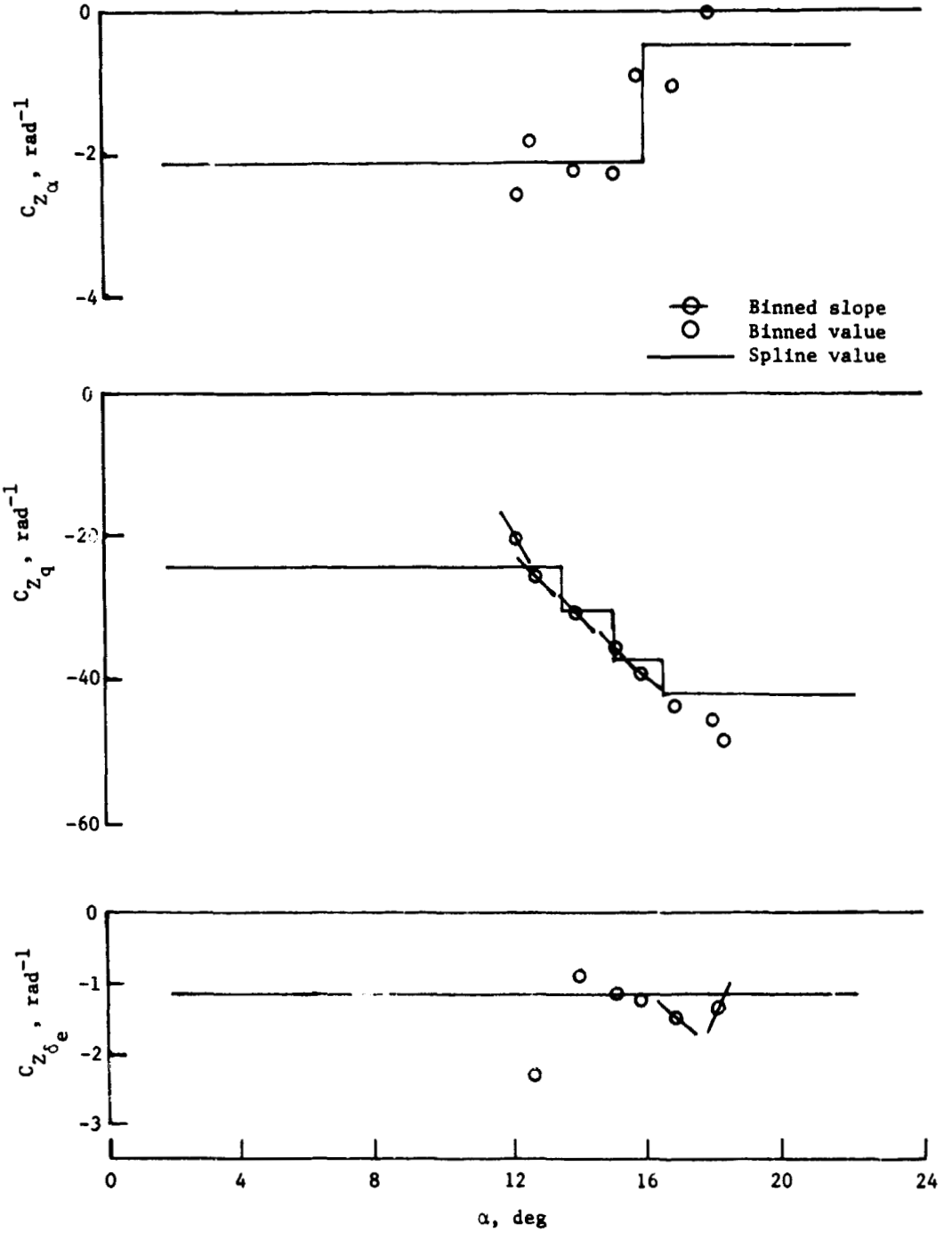

(c) Z-force coefficients for run 7.3.

Figure 8.- Continued.

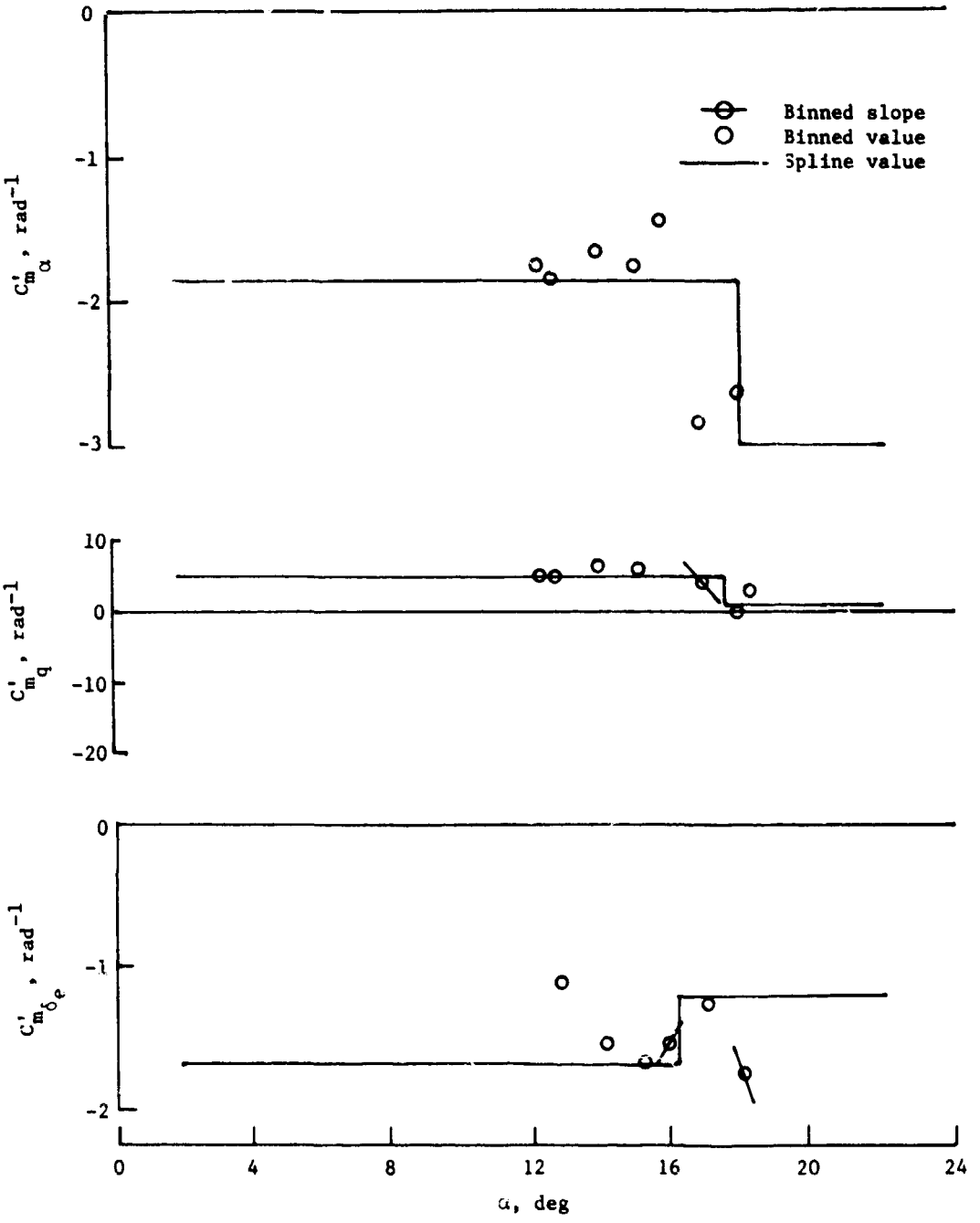

(d) Pitching-moment coefficients for run 7.3.

Figure 8.- Continued.

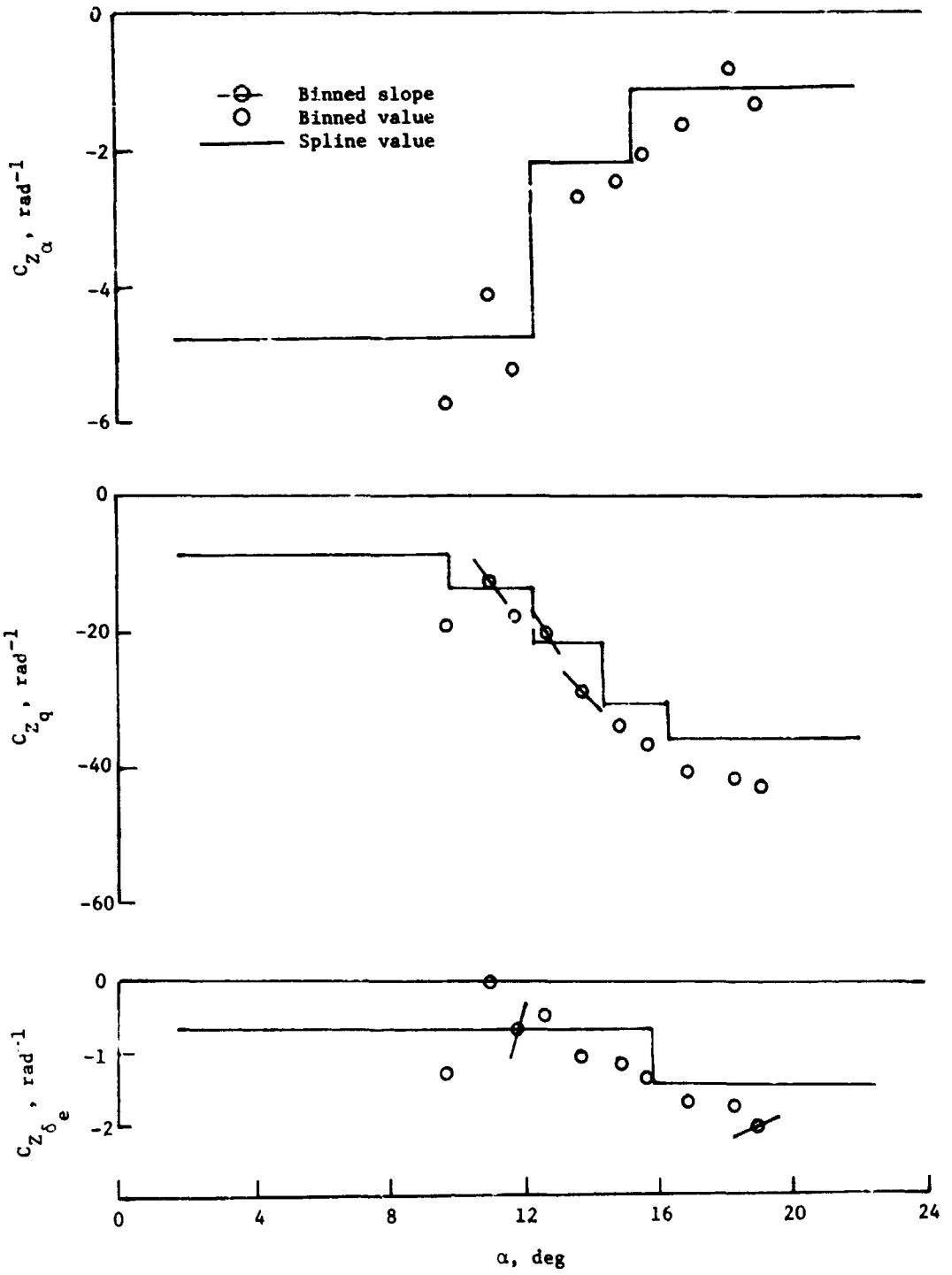

(e) Z-force coefficients for run 7.6.

Figure 8.- Continued.

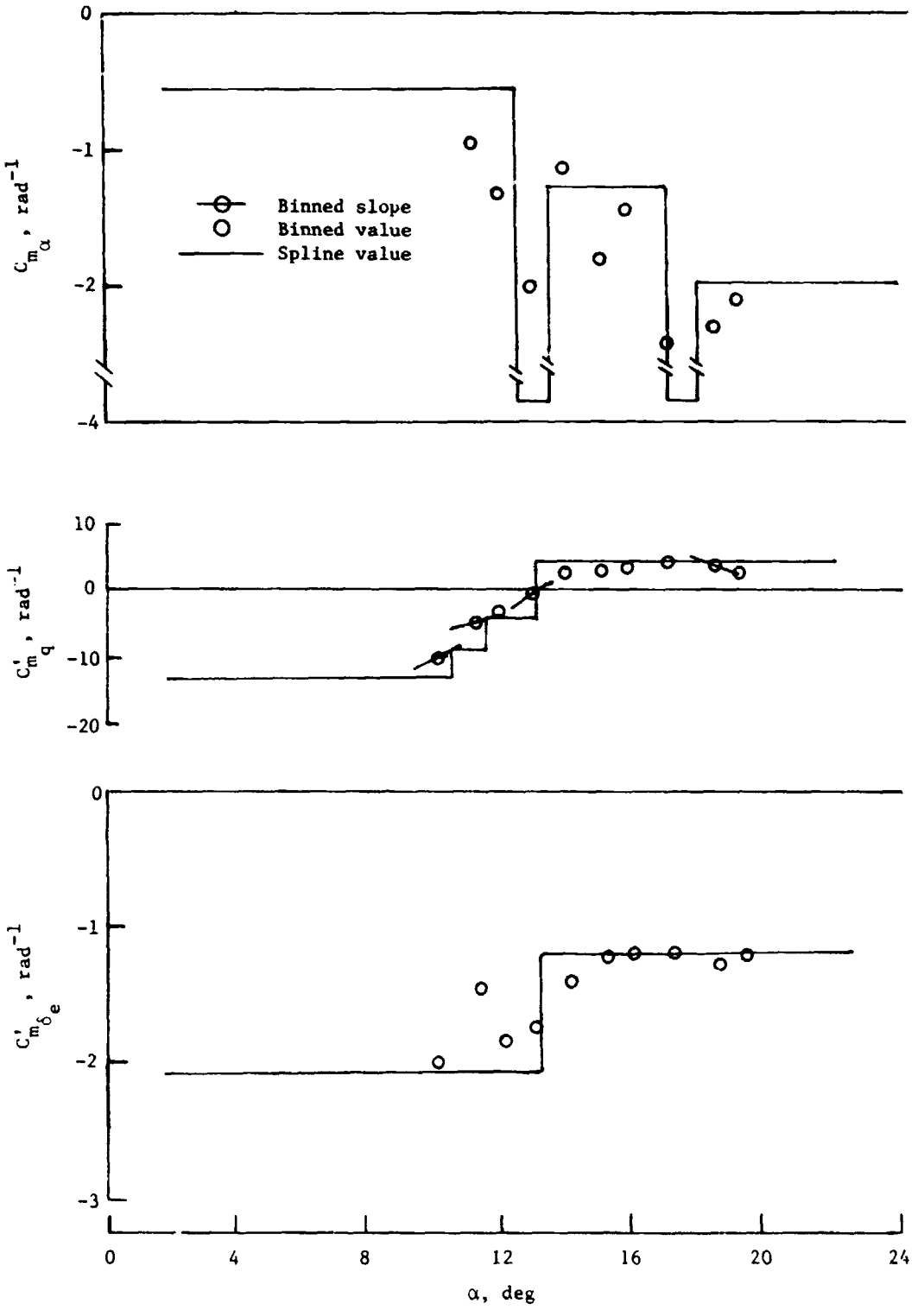

(f) Pitching-moment coefficients for run 7.6.

Figure 8.- Concluded.

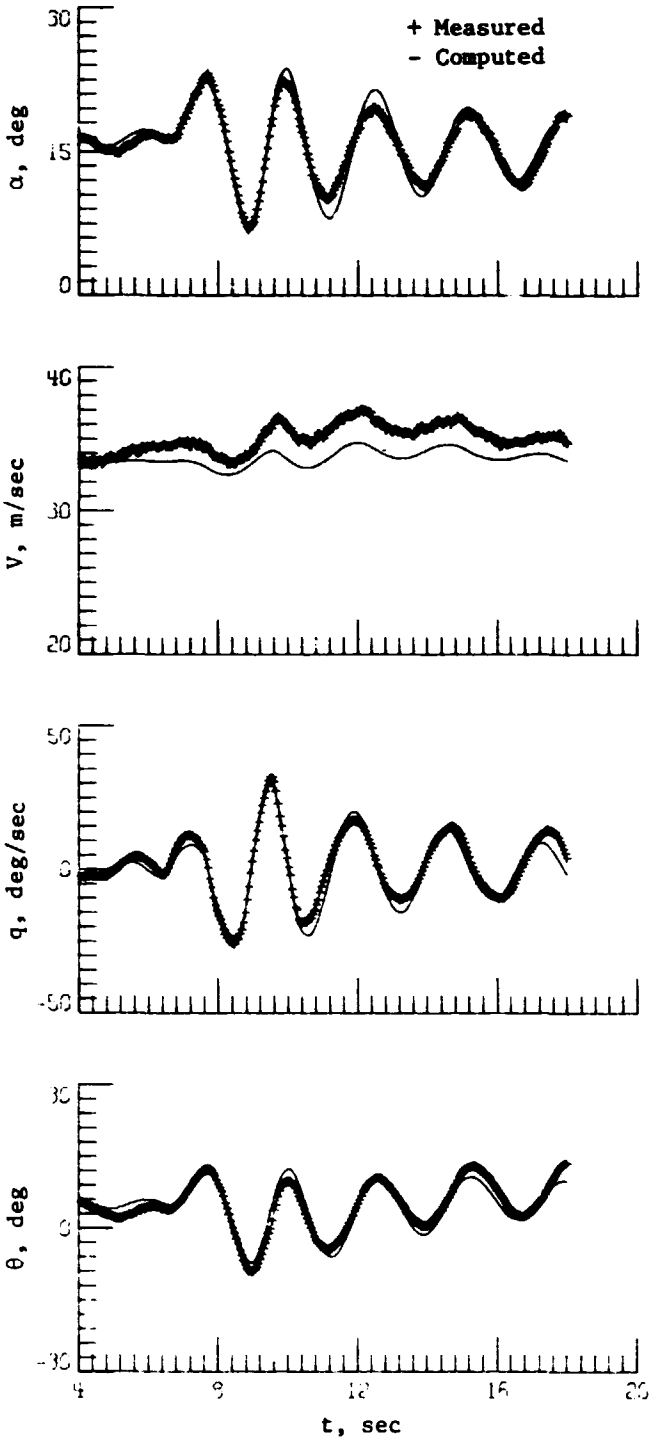

(a) Run 7.1 and linear polynomial model estimated from run 7.1.

Figure 9.- Measured time histories for selected longitudinal variables and those computed from model selected by regression program.

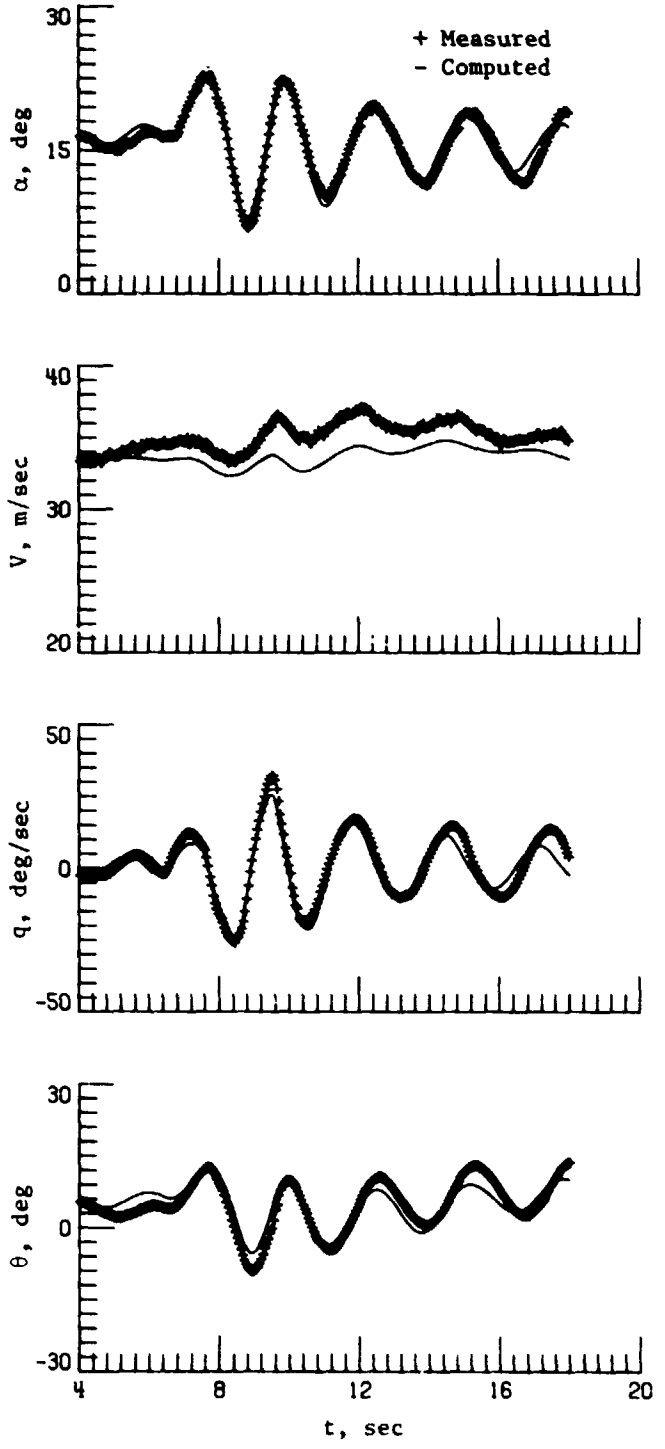

(b) Run 7.1 and spline model estimated from run 7.1.

Figure 9.- Continued.

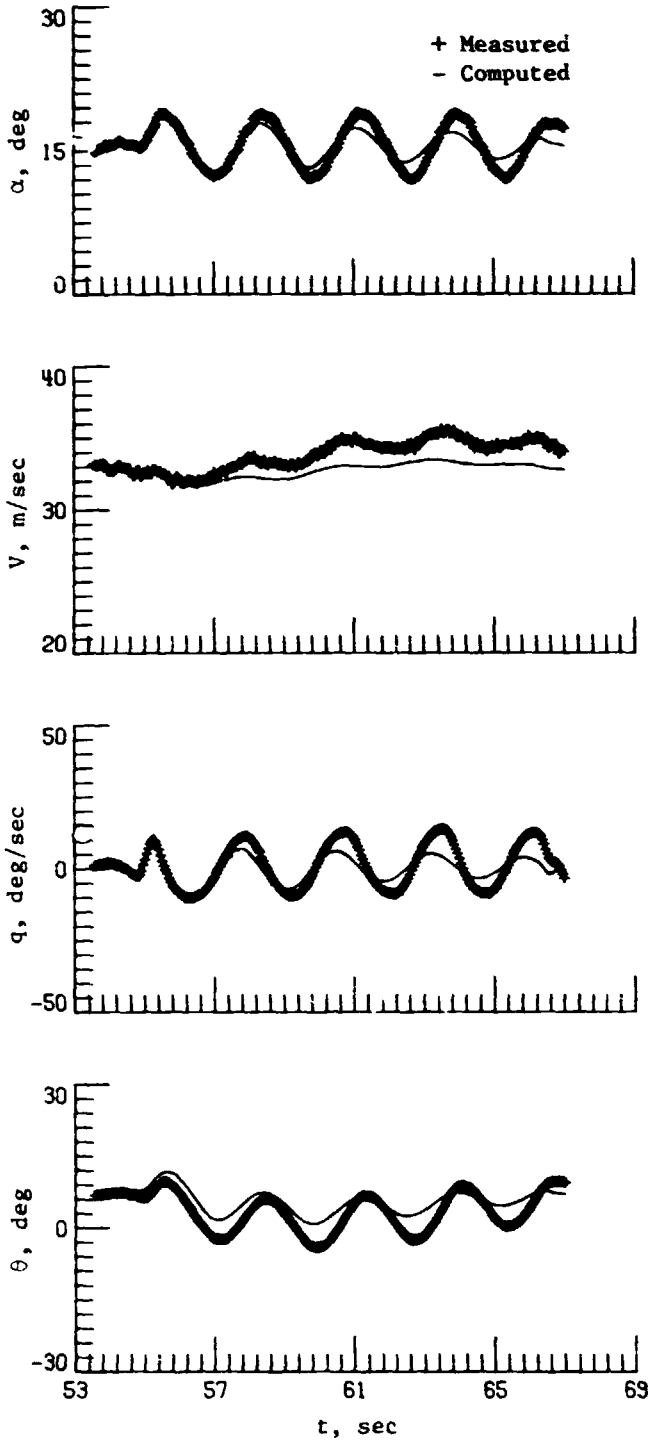

(c) Run 7.3 and spline model estimated from run 7.1.

Figure 9.- Concluded.

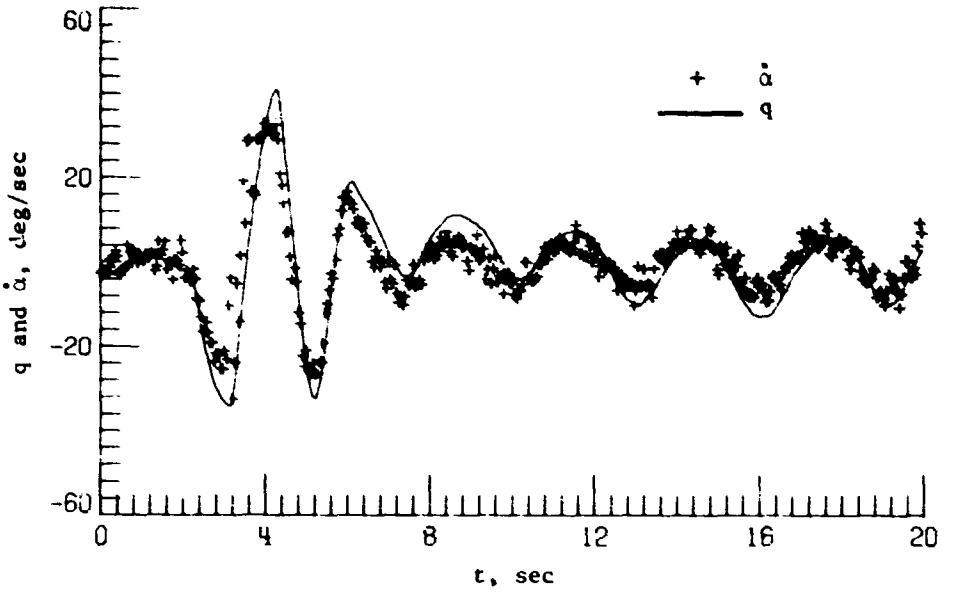

Figure 10.- Time histories of pitch rate and rate of change of angle of attack for an oscillatory run.

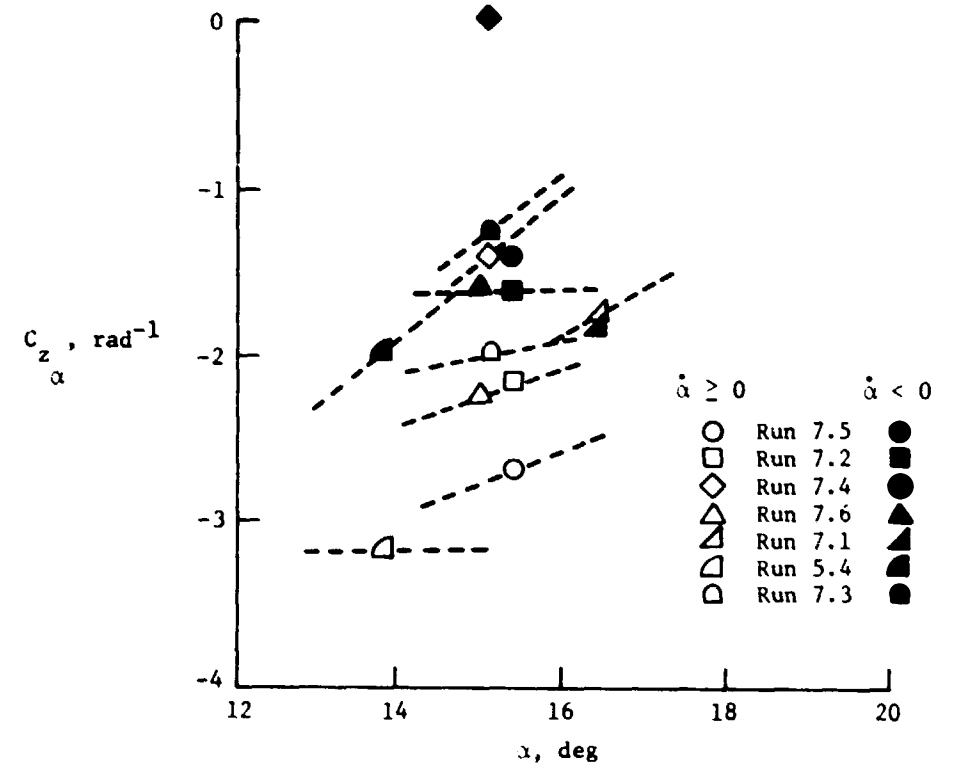

Figure 11.- Values of lift-curve slope for oscillatory runs indicating possibility of lift-curve hysteresis.

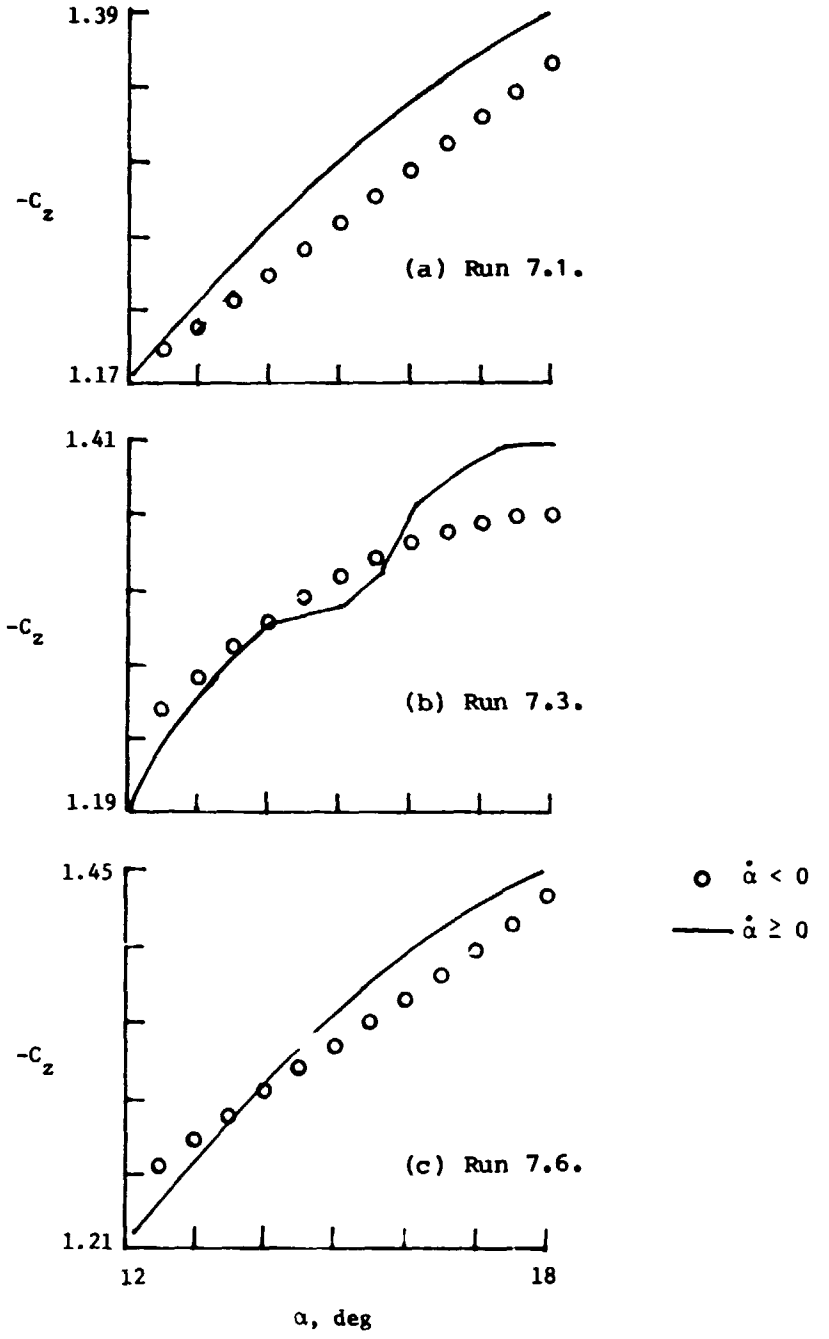

Figure 12.- Plot of lift-curve values estimated by regression applied to data partitioned by rate of change of angle of attack.

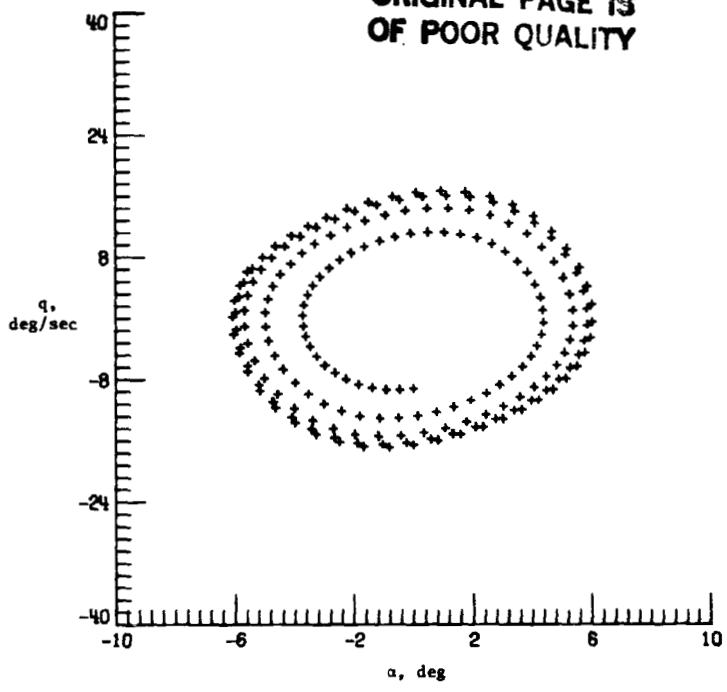

(a) Van der Pol model estimated from run 7.3 showing attainment of limit cycle.

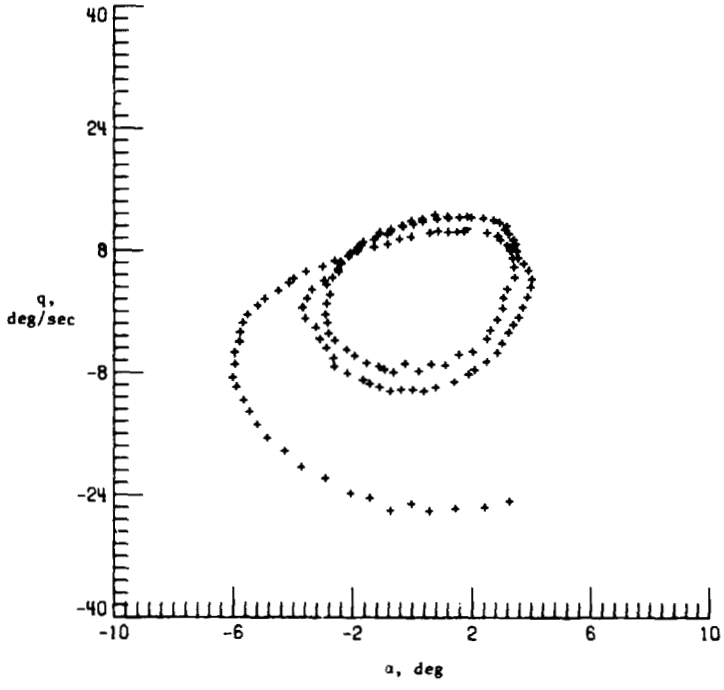

(b) Flight data from run 7.3.

Figure 13.- Phase-plane trajectories of several models and measured data.

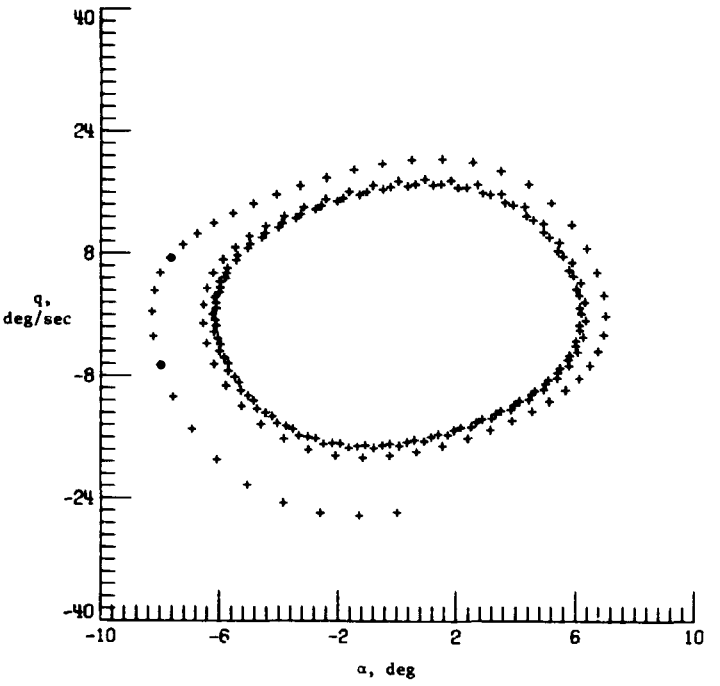

(c) Van der Pol model estimated from run 7.3 showing attainment of limit cycle.

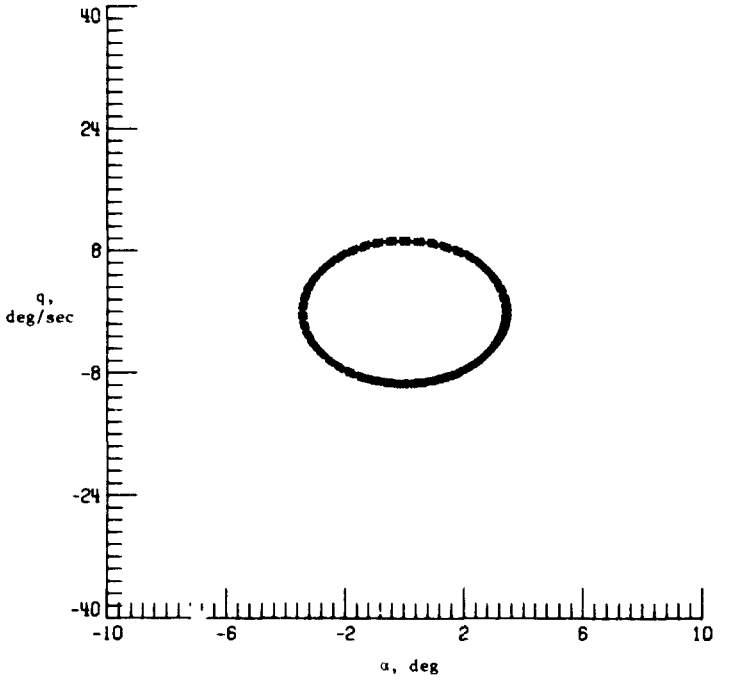

(d) Harmonic oscillator estimated from run 7.3.

Figure 13.- Concluded.